Geoscientific
Model Development

# Isoprene-derived secondary organic aerosol in the global aerosol–chemistry–climate model ECHAM6.3.0–HAM2.3–MOZ1.0

**Scarlet Stadtler[1], Thomas Kühn[2,3], Sabine Schröder[1], Domenico Taraborrelli[1], Martin G. Schultz[1,a], and Harri Kokkola[2]**

[1]Institut für Energie- und Klimaforschung, IEK-8, Forschungszentrum Jülich, Jülich, Germany
[2]Finnish Meteorological Institute, P.O. Box 1627, 70211 Kuopio, Finland
[3]Department of Applied Physics, University of Eastern Finland, P.O. Box 1627, 70211 Kuopio, Finland
[a]now at: Jülich Supercomputing Centre, JSC, Forschungszentrum Jülich, Jülich, Germany

**Correspondence:** Harri Kokkola (harri.kokkola@fmi.fi)

**Abstract.** Within the framework of the global chemistry climate model ECHAM–HAMMOZ, a novel explicit coupling between the sectional aerosol model HAM-SALSA and the chemistry model MOZ was established to form isoprene-derived secondary organic aerosol (iSOA). Isoprene oxidation in the chemistry model MOZ is described by a semi-explicit scheme consisting of 147 reactions embedded in a detailed atmospheric chemical mechanism with a total of 779 reactions. Semi-volatile and low-volatile compounds produced during isoprene photooxidation are identified and explicitly partitioned by HAM-SALSA. A group contribution method was used to estimate their evaporation enthalpies and corresponding saturation vapor pressures, which are used by HAM-SALSA to calculate the saturation concentration of each iSOA precursor. With this method, every single precursor is tracked in terms of condensation and evaporation in each aerosol size bin. This approach led to the identification of dihydroxy dihydroperoxide (ISOP(OOH)2) as a main contributor to iSOA formation. Further, the reactive uptake of isoprene epoxydiols (IEPOXs) and isoprene-derived glyoxal were included as iSOA sources. The parameterization of IEPOX reactive uptake includes a dependency on aerosol pH value. This model framework connecting semi-explicit isoprene oxidation with explicit treatment of aerosol tracers leads to a global annual average isoprene SOA yield of 15 % relative to the primary oxidation of isoprene by OH, $NO_3$ and ozone. With 445.1 Tg (392.1 Tg C) isoprene emitted, an iSOA source of 138.5 Tg (56.7 Tg C) is simulated. The major part of iSOA in ECHAM–HAMMOZ is produced by

IEPOX at 42.4 Tg (21.0 Tg C) and ISOP(OOH)2 at 78.0 Tg (27.9 Tg C). The main sink process is particle wet deposition, which removes 133.6 (54.7 Tg C). The average iSOA burden reaches 1.4 Tg (0.6 Tg C) in the year 2012.

## 1 Introduction

Atmospheric particles play an important role in the earth system, especially in the interactions between climate (IPCC, 2013) and human health (Fröhlich-Nowoisky et al., 2016; Lakey et al., 2016). Aerosols interact with atmospheric radiation directly via absorption and scattering and indirectly via cloud formation. These interactions depend on the particles' microphysical properties, their chemical composition and phase state (Ghan and Schwartz, 2007; Shiraiwa et al., 2017). In the current political debates about air quality and climate change, understanding atmospheric particles is one of the most challenging problems and has led to increased research in this field over the last 2 decades (Fuzzi et al., 2015). Especially organic aerosols are not well understood and subject to ongoing research (Pandis et al., 1992; Kanakidou et al., 2005; Zhang et al., 2007; Fuzzi et al., 2015; Hodzic et al., 2016). Organic aerosol (OA) consists of two types of particles, often mixed and difficult to distinguish (Kavouras et al., 1999; Donahue et al., 2009). First, organic aerosol can be emitted directly into the atmosphere as primary organic aerosol (POA) (Kanakidou et al., 2005; Dentener et al., 2006). Second, organic aerosol mass is also formed from or-

ganic gases emitted as volatile organic compounds (VOCs) and transformed into compounds capable of partitioning into the particle phase. This second type of organic aerosol is called secondary organic aerosol (SOA) (Pankow, 1994; Seinfeld and Pankow, 2003; Jimenez et al., 2009).

Both types of organic aerosols are challenging to model due to limited knowledge about emissions, composition, evolution and physicochemical properties (Lin et al., 2012). Concerning SOA, there are additional uncertainties concerning SOA precursors and the atmospheric chemistry leading to their formation (Heald et al., 2005). Up to now, global models have lacked an explicit treatment of SOA (Zhang et al., 2007) and use relatively simple parameterizations to form SOA, for example the two-product model by Odum et al. (1996). Such parameterizations neglect explicit chemical transformation and assume fixed SOA yields based on laboratory studies (Tsigaridis and Kanakidou, 2003; O'Donnell et al., 2011). Donahue et al. (2006) presented with their volatility basis set (VBS) another approach that allows us to distinguish between various precursor VOCs, but still does not consider the explicit chemical formation and molecular identity of the compounds. The VBS system was further developed to include aerosol aging based on observations of O : C ratio (Donahue et al., 2011). Lin et al. (2012) and Marais et al. (2016) made the first steps into coupling the explicit formation of SOA precursors with SOA formation, focusing on specific compounds.

Global models largely underestimate the amount of atmospheric organic aerosol (Volkamer et al., 2006; De Gouw and Jimenez, 2009; Tsigaridis et al., 2014). This underestimation might be related to the huge number of organic compounds in the atmosphere (Goldstein and Galbally, 2007) that cannot be identified individually by state-of-the-art measuring devices. For explicit modeling, it is necessary to characterize their chemical properties, structures, volatility, solubility and further reaction pathways in the particle phase. Donahue et al. (2009) argue that it is extremely difficult to accomplish dissecting this complexity in detail.

This study makes an attempt to explore the influence of a semi-explicit chemical mechanism by implementing a state-of-the-art isoprene oxidation mechanism, which is based on Taraborrelli et al. (2009, 2012), Nölscher et al. (2014) and Lelieveld et al. (2016), on isoprene-derived secondary organic aerosol (iSOA) formation. Recently, isoprene was identified to contribute to SOA. Literature iSOA yields vary between 1 % and 30 % relative to the total amount of isoprene oxidized by OH, $O_3$ and $NO_3$ (Surratt et al., 2010). Even with a yield as low as 1 %, isoprene as a source of SOA has a huge impact since global annual isoprene emissions are estimated to range between 500 and 750 Tg a$^{-1}$ (Guenther et al., 2006). Therefore, iSOA was investigated in field and laboratory experiments (Claeys et al., 2004; Surratt et al., 2006, 2007a, b). These studies could identify isoprene-derived compounds in the particle phase and identified possible formation pathways (Liggio et al., 2005a; Lin et al., 2013b; Berndt et al.,

2016; D'Ambro et al., 2017a). First-generation products of isoprene are too volatile to partition into the aerosol phase (Kroll et al., 2006); however, they contribute significantly to iSOA formation via heterogeneous and multiphase reactions.

Glyoxal and isoprene epoxide (IEPOX) were identified to undergo reactive uptake and subsequent aqueous-phase reactions (Liggio et al., 2005b; Paulot et al., 2009). Glyoxal uptake might be followed by oligomerization and organosulfate formation depending on aerosol pH value, which is considered to be an irreversible uptake (Liggio et al., 2005a, b). Therefore, glyoxal-derived SOA was studied in different model configurations with reversible and irreversible uptake (Volkamer et al., 2007; Fu et al., 2008; Ervens and Volkamer, 2010; Washenfelder et al., 2011; Waxman et al., 2013; Li et al., 2013).

Experimental and ambient measurements found 2-methyltetrol in the particle phase, which is considered to be formed by IEPOX (Claeys et al., 2004; Paulot et al., 2009; Surratt et al., 2006). Therefore, irreversible reactive uptake from IEPOX was proposed. Surratt et al. (2007b) studied the effect of the pH value on iSOA formation and found the organic carbon mass as a function of aerosol pH. This was studied further, leading to the reaction mechanism for 2-methyltetrol formation from IEPOX to be an acid-catalyzed ring-opening reaction (Eddingsaas et al., 2010; Lin et al., 2013a) and was used to create process parameterizations (Pye et al., 2013; Riedel et al., 2015). Nevertheless, IEPOX uptake was mostly studied in experiments using sulfate aerosol seeds to explore IEPOX uptake dependence on aerosol pH, which leads to the question of whether the reaction might be sulfate catalyzed instead (Surratt et al., 2007a; Xu et al., 2015). However, non-racemic mixtures of tetrol stereoisomers in the atmosphere point to a substantial biological origin (Nozière et al., 2011).

After exploring the IEPOX SOA formation pathway, experimental studies could also identify non-IEPOX SOA formation pathways via the highly oxidized, rather low-volatile isoprene product dihydroxy dihydroperoxide (C5H12O6, ISOP(OOH)2) (Riva et al., 2016; Liu et al., 2016; Berndt et al., 2016; D'Ambro et al., 2017a). This compound was identified under low $NO_x$, meaning $HO_2$-dominated conditions (Berndt et al., 2016) and neutral aerosol pH (Liu et al., 2016; D'Ambro et al., 2017a).

In light of the available knowledge on iSOA formation, this study focuses on iSOA formation via the reactive uptake and explicit partitioning of exclusively semi- and low-volatile isoprene-derived compounds. This paper is organized as follows: Sect. 2 describes the model framework including the sub-models ECHAM6, HAM-SALSA and MOZ. This includes a detailed description of the selection procedure for iSOA precursors and the interplay between the gas-phase oxidation of these and the SALSA aerosol scheme. Furthermore, Sect. 2 describes the model setup and sensitivity runs performed. Section 3 shows the simulation results of the reference run including all iSOA formation pathways,

e.g., global annual budget and mean surface concentrations. Furthermore, additional process understanding is gained by several sensitivity simulations assessing the uncertainties in the reactive uptake of IEPOX, the isoprene oxidation mechanism, the saturation concentration and the evaporation enthalpy. Section 4 discusses possible error sources according to the parameterizations and assumptions used, and Sect. 5 provides conclusions.

## 2 Method

### 2.1 Model description

For this study, the aerosol chemistry climate model ECHAM–HAMMOZ in its version ECHAM6.3–HAM2.3–MOZ1.0 is used (https://redmine.hammoz.ethz.ch/projects/hammoz/wiki/Echam630-ham23-moz10, last access: 9 November 2017; Schultz et al., 2018). This model framework consists of three coupled models. ECHAM6 is the sixth-generation climate model that evolved from the European Center for Medium Range Weather Forecasts (ECMWF) developed at the Max Planck Institute for Meteorology (Stevens et al., 2013). In order to simulate the climate, ECHAM6 solves the prognostic equations for vorticity, divergence, surface pressure and temperature expressed as spherical harmonics with triangular truncation (Stier et al., 2005). All tracers are transported with a semi-Lagrangian scheme on a Gaussian grid (Lin and Rood, 1996). Hybrid $\sigma$–pressure coordinates with a pressure range from 1013 to 0.01 hPa are used for vertical discretization. Aerosol tracers are simulated by the Hamburg Aerosol Model (HAM) with aerosol microphysics based on the Sectional Aerosol module for Large Scale Applications (SALSA) (Kokkola et al., 2008; Bergman et al., 2012; Kokkola et al., 2018). In addition, the chemistry model MOZ simulates atmospheric concentrations of trace gases interacting with aerosols and the climate system (Stein et al., 2012). A detailed description of the HAMMOZ model system is given in Schultz et al. (2018).

For this study SALSA is extended to partition organic trace gases simulated by MOZ between the gas and aerosol phases. Additionally, the isoprene oxidation scheme in the MOZ chemical mechanism was modified in order to model secondary organic aerosol formation. Details can be found in Sect. 2.1.1 and 2.1.2.

Aerosol and trace gas emissions are taken from the ACCMIP interpolated emission inventory (Lamarque et al., 2010). Interactive gas-phase emissions of VOCs are simulated by MEGAN (Model of Emissions of Gases and Aerosols from Nature) (Guenther et al., 2006). For details about the implementation of MEGAN v2.1 in ECHAM–HAMMOZ and its evaluation the reader is referred to Henrot et al. (2017).

For all simulations the triangular truncation 63, leading to a horizontal resolution of $1.875° \times 1.875°$ and 47 vertical layers, is used. The lowest layer thickness corresponding to the surface layer is around 50 m.

### 2.1.1 Chemistry model MOZ

Atmospheric chemistry is simulated by MOZ, solving the chemical equations using an implicit Euler backward solver and treating emissions as well as dry and wet deposition. The current MOZ version evolved from an extensive atmospheric chemical mechanism based on MOZART version 3.5 (Model for Ozone and Related chemical Tracers) (Stein et al., 2012), which merges the tropospheric version MOZART-4 (Emmons et al., 2010) with the stratospheric version MOZART-3 (Kinnison et al., 2007). The chemical mechanism was further developed including a detailed isoprene oxidation scheme based on Taraborrelli et al. (2009, 2012), Nölscher et al. (2014) and Lelieveld et al. (2016) with revised peroxy radical chemistry (Schultz et al., 2018), leading to a model system resembling the CAM-chem model (Community Atmosphere Model with Chemistry) (Lamarque et al., 2010). The chemical mechanism version used here is called JAM3 (Jülich Atmospheric Mechanism version 3). It differs from JAM version 2, evaluated in Schultz et al. (2018), in self- and cross-reactions of isoprene products, added nitrates, initial reactions for monoterpenes and sesquiterpenes, and the production of low-volatile, highly oxidized molecules. The additional isoprene-related reactions can be found in Table S1 in the Supplement. Similar extensions of terpene oxidation are planned; the current study focuses on isoprene. In total 254 gas species are undergoing 779 chemical reactions including 146 photolysis, 16 stratospheric heterogeneous and 8 tropospheric heterogeneous reactions. Thus, the 147 reactions in the semi-explicit isoprene oxidation scheme constitute a substantial fraction of these reactions in JAM3.

In order to identify SOA precursors produced via isoprene oxidation, first, a molecular structure was assigned to each chemical species. Some species are not represented explicitly, but instead they represent groups of compounds with similar chemical properties (lumping). In these cases one structure was assigned to the entire group of isomers. These structures are expressed as SMILES codes in Table 1 and as chemical structures in Fig. 1. Second, with those molecular structures, the saturation vapor pressure $p^*(T)$ of each organic compound in JAM3 was estimated using the group contribution method by Nannoolal et al. (2008) and the boiling point method by Nannoolal et al. (2004) in the framework of the online open source facility UManSysProp (Topping et al., 2016). Third, the group contribution method data were fitted to the Clausius–Clapeyron equation in order to determine the evaporation enthalpy $\Delta H_{vap}$ for each compound. Finally, those species with saturation vapor pressures $p_0^*$ at 298.15 K lower than 0.01 Pa were classified as sufficiently low volatile to take their contribution for SOA forma-

**Table 1.** Isoprene oxidation products in JAM3, physical characteristics and molecular structure expressed as SMILES code. Pure-liquid saturation vapor pressure at the reference temperature 298 K $p_0^*$, Henry's law coefficient H and evaporation enthalpy $\Delta H_{vap}$. $\Delta H_{vap}$ and $p_0^*$ are used in the Clausius–Clapeyron equation for the calculation of the effective saturation vapor pressure as a function of temperature in SALSA. The names of the compounds rely on the Master Chemical Mechanism (MCM 3.2), except for LISOPOOHOOH, which is not in MCM 3.2.

| Compound | SMILES code | $p_0^*$ (298.15 K) (Pa) | $\Delta H_{vap}$ (kJ mol$^{-1}$) | $H$ (mol atm$^{-1}$) |
|---|---|---|---|---|
| LNISOOH | O=CC(O)C(C)(OO)CON(=O)=O* | $2.2 \times 10^{-4}$ | 122.7 | $2.1 \times 10^5$ |
| | CC(O)(CON(=O)=O)C(OO)C=O | $3.8 \times 10^{-4}$ | 120.0 | |
| LISOPOOHOOH | OC(C)(COO)C(CO)OO* | $3.8 \times 10^{-7}$ | 155.3 | $2.0 \times 10^{16}$ |
| | CC(CO)(C(COO)O)OO | $1.9 \times 10^{-7}$ | 158.9 | |
| LC578OOH | OCC(O)C(C)(OO)C=O* | $2.0 \times 10^{-4}$ | 123.2 | $3.0 \times 10^{11}$ |
| | O=CC(O)C(C)(CO)OO | $2.0 \times 10^{-4}$ | 123.2 | |
| C59OOH | OCC(=O)C(C)(CO)OO* | $1.0 \times 10^{-4}$ | 125.0 | $3.0 \times 10^{11}$ |

Names starting with "L" indicate that this species is lumped; SMILES codes of all isomers are shown, but just the ones marked with * are used.
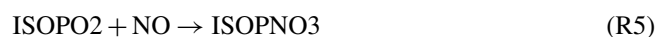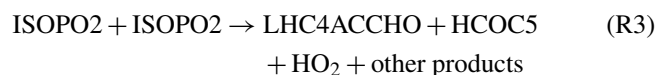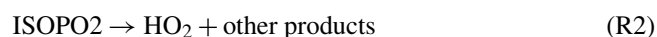
tion into account. This procedure identified four isoprene oxidation products contributing to iSOA formation via gas-to-particle partitioning in ECHAM–HAMMOZ. Table 1 gives the SMILES codes and resulting pure-liquid saturation vapor pressure at the reference temperature $p_0^*$ and the evaporation enthalpy $\Delta H_{vap}$ for all iSOA precursors. The uncertainties in the structure assignment of lumped species and the sensitivity to $\Delta H_{vap}$ are explored in Sect. 3.2.3 and 3.2.4.

Figure 1 shows the chemical pathways of isoprene oxidation and their products to form LIEPOX, LNISOOH, LISOPOOHOOH, LC578OOH and C59OOH. For the whole chemical mechanism including IGLYOXAL formation, the reader is referred to the model description of HAMMOZ in Schultz et al. (2018).

Isoprene-derived SOA precursor gases are formed in MOZ via several reaction steps. Their formation is based on two initial reaction pathways from the oxidation of isoprene by OH and NO$_3$. The O$_3$-initiated reaction pathways are included in MOZ, but the products are too volatile to contribute to SOA formation. The OH-initiated pathway leads to three iSOA precursors called C59OOH, LC578OOH and LISOPOOHOOH in our mechanism. First, OH attacks isoprene C$_5$H$_8$ and forms three isoprene peroxy radical isomers (Reaction R1), and one of them is a lumped species. For simplicity they are called ISOPO2 here.

$$C_5H_8 + OH \rightarrow ISOPO2 \tag{R1}$$

The ISOPO2 isomers either decompose (Reaction R2, Table S1), undergo self- and cross-reactions (Reaction R3, Table S1), or react with ambient radicals, leading to isoprene hydroperoxides (ISOPOOH) (Reaction R4) and isoprene nitrates (ISOPNO3) (Reaction R5).

$$ISOPO2 \rightarrow HO_2 + \text{other products} \tag{R2}$$
$$ISOPO2 + ISOPO2 \rightarrow LHC4ACCHO + HCOC5 \tag{R3}$$
$$+ HO_2 + \text{other products}$$
$$ISOPO2 + HO_2 \rightarrow ISOPOOH \tag{R4}$$
$$ISOPO2 + NO \rightarrow ISOPNO3 \tag{R5}$$

From the reactions of ISOPOOH with OH a hydroperoxide peroxy radical is formed: a lumped species called LISOPOOHO2 (Reaction R6).

$$ISOPOOH + OH \rightarrow \alpha \cdot LISOPOOHO2 + \beta \cdot LIEPOX + \beta \cdot OH \tag{R6}$$

It can be oxidized by HO$_2$ to LISOPOOHOOH (Reaction R7). The stoichiometric coefficients $\alpha$ and $\beta$ vary depending on the ISOPOOH isomer that is oxidized. These stoichiometric coefficients can be found in Table S2.

$$LISOPOOHO2 + HO_2 \rightarrow LISOPOOHOOH \tag{R7}$$

Not included in the JAM3 reference case is the 1,5-H shift of LISOPOOHO2 that yields compounds with a higher volatility than LISOPOOHOOH (D'Ambro et al., 2017b), so the chemical yield of LISOPOOHOOH is expected to be an upper limit. D'Ambro et al. (2017b) estimated the rate of the 1,5-H shift of LISOPOOHO2 to be higher than 0.1 s$^{-1}$. For this reason, the suggested product, an epoxide, might be more prevalent than LISOPOOHOOH, but still lead to a substantial amount of iSOA via a similar heterogeneous reactive uptake like for IEPOX. The importance of LISOPOOHOOH and LISOPOOHO2 isomerization is discussed in Sect. 3.2.5, in which the impact of the 1,5-H shift of LISOPOOHO2 is included in JAM3 and tested in two sensitivity simulations. Reactions (R1)–(R7) show that LISOPOOHOOH production
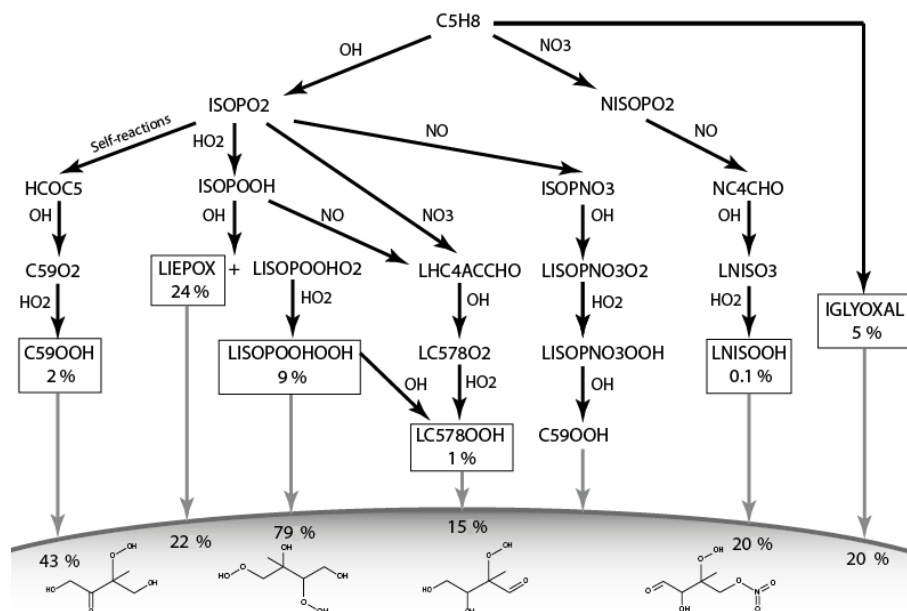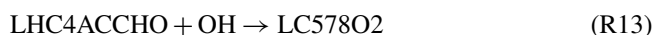
**Figure 1.** Simplified overview of chemical pathways leading to sufficiently low-volatile isoprene-derived compounds able to partition into the aerosol phase. Note that ISOPO2 is used here for simplicity; JAM3 includes three different ISOPO2s (LISOPACO2, ISOPBO2, ISOPDO2), and the same applies for ISOPOOH. The percentages in the boxes indicate average mass yields and thus the annual mean reaction turnover of isoprene leading to these products. For IGLYOXAL there are too many formation pathways and they are therefore not shown. The solid horizontal curve represents the boundary to the particle phase. Percentages found under the corresponding arrow express the annual mean individual net iSOA yield of the compound. Except for LIEPOX and IGLYOXAL, structures are relevant to estimate the saturation vapor pressure and evaporation enthalpy and are therefore shown here. For the detailed mechanism, the reader is referred to Schultz et al. (2018).

depends on ambient radical concentrations, and thus it varies in space and time. On global annual average for 2012, the chemical mass yield of LISOPOOHOOH is 9 %. This means that 9 % of the total carbon mass emitted in 2012 as isoprene ended up as LISOPOOHOOH. LISOPOOHOOH can either react back to LISOPOOHO2 or be photolyzed or oxidized by OH to form LC578OOH (Reaction R8).

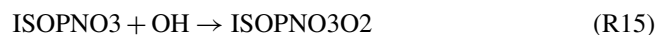$$\text{LISOPOOHOOH} + \text{OH} \rightarrow \text{LC578OOH} + \text{OH} \tag{R8}$$

LC578OOH is a lumped species representing two MCM species: C57OOH and C58OOH. LC578OOH is more volatile than LISPOOHOOH and can be formed via another pathway as well.

$$\text{ISOPO2} + \text{NO} \rightarrow \text{LHC4ACCHO} + \text{NO}_2 \tag{R9}$$
$$\text{ISOPO2} + \text{NO}_3 \rightarrow \text{LHC4ACCHO} + \text{NO}_2 \tag{R10}$$
$$\text{ISOPNO3} + h\nu \rightarrow \text{LHC4ACCHO} + \text{NO}_2 + \text{HO}_2 \tag{R11}$$
$$\text{ISOPOOH} + h\nu \rightarrow \text{LHC4ACCHO} + \text{OH} + \text{HO}_2 \tag{R12}$$
$$\text{LHC4ACCHO} + \text{OH} \rightarrow \text{LC578O2} \tag{R13}$$
$$\text{LC578O2} + \text{HO}_2 \rightarrow \text{LC578OOH} \tag{R14}$$

Reactions (R9)–(R14) show LC578OOH formation via LHC4ACCHO degradation. LHC4ACCHO is a lumped species representing the MCM species HC4ACHO and HC4CCHO. Finally, LHC4ACCHO is oxidized by OH (Reaction R13) and forms LC578O2, which reacts with HO2

to LC578OOH (Reaction R14). LC578OOH either reacts with OH back to LC578O2 or is photolyzed. LC578O2 can undergo a 1,4 H shift and recycle OH, like RO$_2$ from methacrolein (Crounse et al., 2011). On global annual average for 2012, just 1 % of the oxidation of total isoprene carbon mass leads to LC578OOH.

The third compound formed from the OH-initiated oxidation of isoprene is C59OOH. Starting from ISOPO2, there are two possible oxidation ways for C59OOH formation, one with nitrates as intermediates and a second one in which nitrogen oxide is not required. The nitrate pathway starts with the formation of ISOPNO3 from ISOPO2 (R5) and continues with OH reaction to form isoprene nitrate peroxy radicals ISOPNO3O2 (Reaction R15), which is again a lumped species.

$$\text{ISOPNO3} + \text{OH} \rightarrow \text{ISOPNO3O2} \tag{R15}$$
$$\text{ISOPNO3O2} + \text{CH3O2} \rightarrow \text{ISOPNO3OOH} \tag{R16}$$
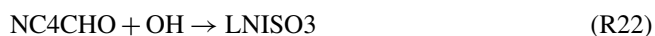$$\text{ISOPNO3OOH} + \text{OH} \rightarrow \text{C59OOH} \tag{R17}$$

Via the formation of a nitrate hydroxyperoxy radical, finally C59OOH is formed (Reaction R17). This pathway requires the availability of NO for the initial step in (Reaction R5). For the second pathway, no NO is needed.

$$HCOC5 + OH \rightarrow C59O2 \tag{R18}$$

$$C59O2 + HO_2 \rightarrow C59OOH \tag{R19}$$

Self-reactions of ISOPO2 (Reaction R3) lead to the formation of HCOC5, which is then converted via OH to C59O2 (Reaction R18). $HO_2$ oxidizes C59O2 to C59OOH (Reaction R19). C59OOH can also react back to C59O2 or be lost via photolysis. The overall annual average mass yield from isoprene to C59OOH is 2 %.

The fourth iSOA precursor is an isoprene-derived nitrate LNISOOH, which requires both a $NO_x$-dominated and an $HO_2$-dominated environment because only the first two oxidation steps use nitrate; then OH and $HO_2$ are required. First, isoprene reacts with the $NO_3$ radical and forms a nitrate peroxy radical NIOSPO2 (Reaction R20), which oxidizes NO and forms NC4CHO (Reaction R21). NC4CHO, in contrast, has to react with OH to form LNISO3 (Reaction R22), which then reacts with $HO_2$ and forms LINSOOH (Reaction R23).

$$C_5H_8 + NO_3 \rightarrow NISOPO2 \tag{R20}$$

$$NISOPO2 + NO \rightarrow NC4CHO \tag{R21}$$

$$NC4CHO + OH \rightarrow LNISO3 \tag{R22}$$

$$LNISO3 \rightarrow LNISOOH \tag{R23}$$

LNISOOH can be photolyzed or react back to LNISO3. The fact that LINISOOH formation requires an environment in which first NO dominates chemistry followed by $HO_2$ limits its formation in the atmosphere. It is formed in small amounts, and therefore on annual mean, the oxidation of isoprene in 2012 yields only 0.1 % LNISOOH.

In Fig. 1, a simplified overview of the described chemical reactions can be found. MOZ calculates branching ratios according to ambient conditions, and the gas-phase yields shown in Fig. 1 result from a global perspective. These gas-phase yields are the resulting annual averages for 2012 and not fixed yields. Accordingly, the particle-phase yields result from volatility or reactive uptake parameterization from the corresponding iSOA precursors. These yields are not fixed either, but are calculated from the global annual average for the year 2012.

To cover multiphase chemical iSOA formation, heterogeneous reactions on aerosols of IEPOX and isoprene-derived glyoxal were included. Nevertheless, ECHAM–HAMMOZ does not include in-particle or in-cloud aqueous-phase chemistry, and therefore no assumptions of in-particle products are made. Furthermore, no SOA formation via cloud droplets is included in ECHAM–HAMMOZ due to constraints in the aerosol–cloud interaction formulation. Therefore, reactive uptake is parameterized as pseudo-first-order loss using aerosol surface area density given by HAM, according to Schwartz (1986) and described in detail in Stadtler et al. (2018a).

In MOZ, three IEPOX isomers are lumped together (LIEPOX) and the compound IGLYOXAL was introduced to differentiate between isoprene-derived glyoxal and glyoxal from other sources. Isoprene glyoxal formation pathways are numerous and no changes were made to the mechanism with respect to IGLYOXAL formation. Since these reactions are included also in JAM2, see Schultz et al. (2018). LIEPOX is formed along the pathway described for LISPOOHOOH in Reaction (R6).

Glyoxal is observed to produce a variety of compounds, like oligomers or organosulfates, in the aqueous aerosol phase and glyoxal is capable of being released back into the gas phase (Volkamer et al., 2007; Ervens and Volkamer, 2010; Washenfelder et al., 2011; Li et al., 2013). The simplification assuming irreversible uptake might thus overestimate its impact on iSOA. Following previous model studies (Fu et al., 2008; Lin et al., 2012) a reaction probability of $\gamma_{glyoxal} = 2.9 \times 10^{-3}$ (Liggio et al., 2005b) is used.

For IEPOX the irreversibility is a less critical assumption because IEPOX forms 2-methyltetrol and organosulfates in the aqueous aerosol phase, which stay in the aerosol phase (Claeys et al., 2004; Eddingsaas et al., 2010; Lal et al., 2012; McNeill et al., 2012; Woo and McNeill, 2015). However, ECHAM–HAMMOZ does not include explicit treatment of aqueous-phase reactions. The reaction probability of IEPOX varies with pH value (Lin et al., 2013a; Pye et al., 2013; Gaston et al., 2014), which cannot be captured by ECHAM–HAMMOZ due to the lack of ammonium and nitrate in the aerosol phase and thus the possibility to capture aerosol pH. For these reasons, the reaction probability of IEPOX $\gamma_{IEPOX} = 1 \times 10^{-3}$ (Gaston et al., 2014) was chosen, close to the value used by Pye et al. (2013). To explore the impact of pH dependence, sensitivity runs with different $\gamma_{IEPOX}$ are analyzed. Additionally, no assumptions of in-particle products are made, and in ECHAM–HAMMOZ IEPOX is simply taken up into the aerosol phase without further transformation.

### 2.1.2 HAM-SALSA

The Hamburg Aerosol Model (HAM) handles the evolution of atmospheric particles and includes emissions, removal, microphysics and radiative effects. Moreover, the current configuration uses the Sectional Aerosol module for Large Scale Applications (SALSA) for the calculation of aerosol microphysics (Kokkola et al., 2008, 2018). In SALSA the aerosol size distribution is divided into aerosol size sections (size bins). Furthermore, these size bins are grouped into subranges, which allows the model to limit the computation of the aerosol microphysical processes to include only the aerosol sizes that are relevant. Microphysical processes simulated by SALSA cover nucleation, condensation, coagulation, cloud activation, sulfate production and hydration (Bergman et al., 2012). The aerosol composition is described using five different aerosol compounds: sulfate, black carbon, dust, sea salt and organic carbon. Furthermore, SALSA treats secondary organic aerosol formation via the volatil-

**Table 2.** Description of simulations performed.

| Simulation | Description | Simulation period |
|---|---|---|
| RefBase | Reference run with uniform reaction probabilities for IEPOX and isoprene glyoxal $\gamma_{\text{IEPOX}} = 1.0 \times 10^{-3}$, $\gamma_{\text{IGYOXAL}} = 2.9 \times 10^{-3}$ (see Sect. 2.1.1), partitioning precursor $\Delta H_{\text{vap}}$ and $p_0^*$ (298.15 K) given in Table 1 | Whole year 2012 |
| RefVBS | ECHAM–HAM simulation with VBS approach and pseudo-chemistry (see Sect. 2.1.2) | June, July, August 2012 |
| $\Delta H_{30}$ | Like RefBase, but with same $\Delta H_{\text{vap}} = 30\,\text{kJ mol}^{-1}$ for all compounds | June, July, August 2012 |
| EVA | Like RefBase, but with $\Delta H_{\text{vap}}$ and $p_0^*$ derived with EVAPORATION (Compernolle et al., 2011) instead of Nannoolal et al. (2008) method | Whole year 2012 |
| $\gamma$pH | Like RefBase, but with $\gamma_{\text{IEPOX}} = f(\text{pH})$ | June, July, August 2012 |
| HshiftIEP | Additional reaction in JAM3 (Reaction R24) | June, July, August 2012 |
| HshiftLC5 | Additional reaction in JAM3 (Reaction R25) | June, July, August 2012 |
| DECAY | LISOPOOHOOH in-particle decay | June, July, August 2012 |
| JPHOT | SOA photolysis with $J_{\text{SOA}} = 0.004\,\%\,J_{\text{NO}_2}$ | June, July, August 2012 |

ity basis set (Kühn et al., 2018). In the model setup described there, SALSA uses a strongly simplified description for VOC oxidation (pseudo-chemistry) to obtain SOA precursors. Here, the model system was extended and coupled to MOZ, which explicitly calculates SOA precursors as described in Sect. 2.1.1. The standard SALSA-VBS system is not used here. Instead for each SOA-forming compound the gas-to-particle partitioning is treated explicitly and its concentration is tracked in both the gas and the aerosol phases separately. This study exclusively uses isoprene-derived precursors to form iSOA, and other oxygenated compounds capable of partitioning derived from terpenes or aromatics are neglected.

### 2.1.3 Coupling of HAM-SALSA and MOZ

HAM-SALSA and MOZ interact through several processes, and oxidation fields calculated by MOZ are passed to HAM-SALSA for aerosol oxidation, MOZ produces $H_2SO_4$, which is then converted by HAM-SALSA to sulfate aerosol and HAM-SALSA provides the aerosol surface area density for heterogeneous chemistry. Above all, HAM-SALSA takes the information of iSOA precursor gas-phase concentrations and their physical properties to calculate the saturation concentration coefficient ($C^*$) using the Clausius–Clapeyron equation (Eq. 1) (Farina et al., 2010).

$$C_i^* = C_i^*(T_0)\frac{T_0}{T}\exp\left[\frac{\Delta H_{\text{vap}}}{R}\left(\frac{1}{T_0} - \frac{1}{T}\right)\right] \qquad (1)$$

Here $T_0$ is the reference temperature of 298.15 K and $\Delta H_{\text{vap}}$ is the evaporation enthalpy given in Table 1 for the iSOA precursors identified in this study. $C^*$ is then used to calculate the explicit partitioning of the iSOA precursors to each aerosol section. This process is reversible and it is thus possible that the iSOA formed in one region is transported and evaporates in another region. Explicitly calculating the partitioning instead of prescribing yields in chemical production or SOA formation is a key difference to other models

with fixed yields. Loss processes for SOA in HAM-SALSA include sedimentation, deposition and washout in the aerosol phase.

### 2.2 Simulation setup and sensitivity runs

An overview of the performed simulations can be found in Table 2. The reference simulation RefBase, which includes a 3-month spin-up and spans the time from October 2011 until the end of December 2012, is evaluated for the entire year 2012, while sensitivity runs are usually limited to the northern hemispheric, isoprene-emission-intense summer season of June, July and August.

Several sensitivity simulations were performed to explore model sensitivities and assess uncertainties. For comparison of the explicit ECHAM–HAMMOZ scheme to a state-of-the-art VBS scheme, ECHAM–HAM with pseudo-chemistry and VBS configuration (RefVBS), as described in Sect. 2.1.2, was run. $\Delta H_{30}$ uses the same, much lower evaporation enthalpy of $\Delta H_{\text{vap}} = 30\,\text{kJ mol}^{-1}$ for all partitioning species following Farina et al. (2010). The uncertainty in the saturation vapor pressure estimation method was assessed by comparing the Nannoolal et al. (2008) method to the EVAPORATION (Compernolle et al., 2011) method.

Furthermore, the pH value dependence of IEPOX is tested in $\gamma$IEX, formulating an easy pH-dependent parameterization based on laboratory measurements. Particle pH values cannot be obtained from ECHAM–HAMMOZ itself as the model does not include the calculation of particle-phase thermodynamics. For this reason, aerosol pH was calculated offline using the AIM aerosol thermodynamics model (Clegg et al., 1998). The SALSA-simulated annual mean mass of aerosol water and the mean mass of aerosol-phase inorganic compounds at the lowest model level were used an input for AIM. This required three additional assumptions: (1) all aerosol is in liquid form, (2) liquid water content is affected by all hygroscopic compounds, but only sulfate is assumed to affect the activity of the hydrogen ion (i.e., aerosol pH), and
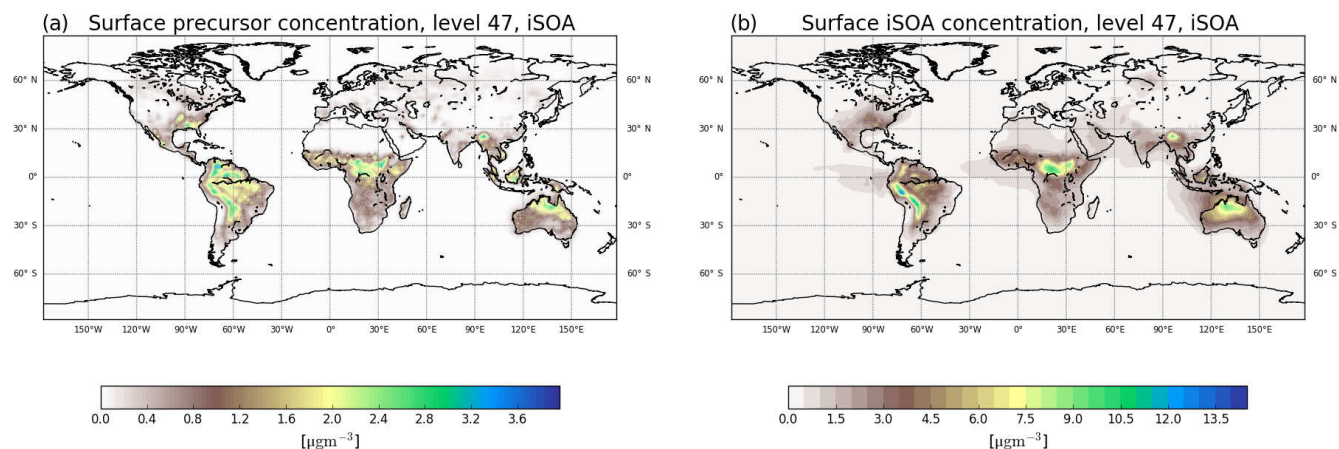
2012-07-16 11:52



**Figure 2.** Global surface layer maps showing the iSOA precursor gas-phase concentration in (**a**) and the aerosol-phase iSOA concentration in (**b**) as annual averages for 2012 in $\mu g\,m^{-3}$. The reader should note the different color scales; higher concentrations are reached in the aerosol phase (**b**).

(3) all sulfate is in the form of ammonium bisulfate. This second assumption for sulfate has to be done because particle-phase ammonia is not modeled in the current configuration of ECHAM–HAMMOZ. Using these inputs, AIM provided the concentration of the hydrogen ion ($H^+$) as an output. The resulting, global aerosol pH values thus vary strongly by region according to the RH and can be found in Fig. S1 in Supplement 2.

As described in Sect. 2.1.1, JAM3 does not include the 1,5-H shift reaction of LISOPOOHO2. D'Ambro et al. (2017b) describe the product resulting from the 1,5-H shift reaction of LISOPOOHO2, a compound that is a highly oxidized epoxide. This compound is missing in ECHAM–HAMMOZ, and thus the 1,5-H shift reaction was introduced as follows.

The structure of the compound described in D'Ambro et al. (2017b) relates to a compound that possibly undergoes reactive uptake as IEPOX, but at the same time looks semi-volatile like LC578OOH. For this reason, two simulations for the time period June, July and August 2012 were performed, one including Reaction (R24).

$$\text{LISOPOOHO2} \rightarrow \text{LIEPOX} \tag{R24}$$

A second simulation included Reaction (R25) instead of Reaction (R24). Both reactions use the best estimate for the reaction coefficient of $0.3\,s^{-1}$ (D'Ambro et al., 2017b). No temperature dependence was included.

$$\text{LISOPOOHO2} \rightarrow \text{LC578OOH} \tag{R25}$$

To explore in-particle loss and SOA photolysis, short test runs including these processes were performed (DE-CAY and JPHOT). In-particle loss is formulated as simple LISOPOOHOOH decay with a half-life of 4 h (D'Ambro

et al., 2017a; Stadtler, 2018). SOA photolysis is formulated as described in detail in Hodzic et al. (2015), but using a weaker photolysis frequency of 0.004 % $J_{NO_2}$. This lower SOA photolysis frequency was chosen to take the argumentation by Malecha and Nizkorodov (2016) into account that in-particle photolysis is weaker than gas-phase photolysis due to stabilization of the molecules in the particle.

## 3  Results

### 3.1  Reference run RefBase

#### 3.1.1  Global distributions

Figure 2 shows the annual mean surface concentrations for total iSOA and its precursors in the gas phase. The precursors are formed, except for LNISOOH, during daytime and build up quickly. Therefore, these are found very close to isoprene source regions mostly in the tropics and Southern Hemisphere. Their highest values, up to $3\,\mu g\,m^{-3}$, are simulated over the Amazon, the east flank of the Andes, Central Africa, northern Australia, Indonesia and Southeast Asia. In the annual mean also the northern hemispheric summer is visible, but peak values of over $2\,\mu g\,m^{-3}$ are only reached on Mexico's west coast and in the southeastern US. In Europe and northern Asia, where isoprene emissions are much lower, mean values up to $0.5\,\mu g\,m^{-3}$ for precursors are calculated.

These low precursor concentrations correspond to the very low iSOA concentrations over Europe and northern Asia compared to the southeastern US and Mexico's west coast, where up to $4.5\,\mu g\,m^{-3}$ iSOA is formed. The highest iSOA concentrations are found where high precursor concentrations meet preexisting aerosol, like in Central Africa be-

cause of it high biomass burning emissions or Southeast Asia where aerosol pollution is high. In the latter, ECHAM–HAMMOZ simulates values of up to $13\,\mu g\,m^{-3}$ iSOA. The Amazon is a region of very high isoprene emissions and therefore high iSOA precursor concentrations; nevertheless, the local maximum in iSOA of $13.5\,\mu g\,m^{-3}$ can be seen on the east side of the Andes. This pattern is caused by pre-existing aerosol, which in ECHAM–HAMMOZ tends to accumulate on the east side of the Andes, and the still high iSOA precursor concentrations in the same region. Also in the northern part of Australia higher precursor loadings are found, leading to iSOA ground-level concentrations of up to $9\,\mu g\,m^{-3}$ there.

It can also be seen that iSOA has a longer lifetime than its gas-phase precursors. Prevailing wind directions are recognizable, clearly showing the transport of iSOA over the oceans, for example in the South American and African outflow regions. Also, iSOA is transported from Australia to the north. The average iSOA lifetime was calculated to be around 4 days, so long-range transport is limited before iSOA is lost due to wet deposition (see Sect. 3.1.2).

Farina et al. (2010) included iSOA formation with fixed yields of isoprene transformation to the different VBS classes and also showed its global annual surface distribution for 1979–1980. Compared to Farina et al. (2010) ECHAM–HAMMOZ simulates nearly 1 order of magnitude higher maximum iSOA concentrations. This is explained by much higher reaction turnover from MOZ leading to higher amounts of iSOA precursors than produced by the low yields prescribed in Farina et al. (2010). The global patterns agree on high values over the southeastern US, South America, Central Africa and northern Australia. In contrast, Farina et al. (2010) do not simulate the maximum over Southeast Asia. Hodzic et al. (2016) show biogenic SOA for the lower 5 km on a global scale, and again general patterns agree with the distribution in ECHAM–HAMMOZ. Nevertheless, Hodzic et al. (2016) simulated higher concentrations over Eurasia, which is not captured by ECHAM–HAMMOZ due to the lack in other biogenic VOC-derived SOA.

Total biogenic SOA concentrations compare well with iSOA surface concentrations of ECHAM–HAMMOZ within their order of magnitude, which again underlines the higher yields in ECHAM–HAMMOZ. High concentrations result from the highly oxidized compounds produced by MOZ chemistry, especially due to LISOPOOHOOH, which has a molar mass of $168.14\,\mathrm{g\,mol^{-1}}$ that is very large. LISOPOOHOOH and LIEPOX contribute most to iSOA, followed by isoprene glyoxal. To further discuss this, iSOA composition concentrations for northern hemispheric summer (June, July, August) are shown in Fig. 3.

Figure 3a, c, e and g show gas-phase precursor concentrations and Fig. 3c, d, f and g show particle-phase concentrations. First, LIEPOX (panels a, b) and LISOPOOHOOH (panels c, d) are shown because they have greatest impact in the particle phase, followed by IGLYOXAL (panels e, f). The other iSOA precursors are shown together because of their low concentrations in the gas (panel g) and particle phase (panel h). On the right-hand side corresponding mean values in the particle phase are displayed.

From the gas-phase LIEPOX distribution (Fig. 3a) it can be seen that MOZ simulates concentrations of around $0.5\,\mu g\,m^{-3}$ over isoprene-rich areas. Peak values of $4.5\,\mu g\,m^{-3}$ LIEPOX are found over the southeastern US, north Venezuela and north of Myanmar. Higher concentrations of LIEPOX are reached in the aerosol phase. For example, in South America gas-phase concentrations vary between 1.5 and $2.5\,\mu g\,m^{-3}$, but LIEPOX SOA values over $7\,\mu g\,m^{-3}$ are reached on the eastern edge of the Andes. LIEPOX SOA transport over the ocean and over the Sahara can particularly be seen. No assumption of in-particle products for LIEPOX was made, but usually 2-methyltetrols are present in $ng\,m^{-3}$ concentrations in the particle phase (Claeys et al., 2004; Kourtchev et al., 2005; Clements and Seinfeld, 2007). Lopez-Hilfiker et al. (2016) report that 80 % of IEPOX forms dimers instead of 2-methyltetrols, which would increase the concentrations of IEPOX-derived SOA in the ambient measurements. Accounting additionally for these 80 %, the mass concentrations would reach around $10–100\,ng\,m^{-3}$, and still an overestimation of simulated LIEPOX SOA is indicated.

In contrast to LIEPOX, LISOPOOHOOH gas-phase concentrations (Fig. 3c) are very low and even with a scale focusing on low values, these cannot be captured on a scale fitting to the other compounds. For gas-phase LISOPOOHOOH global values lower than $0.1\,\mu g\,m^{-3}$ are calculated. This is a consequence of iSOA formation. Figure 3d shows that LISOPOOHOOH SOA appears in high concentrations between 1 and $8\,\mu g\,m^{-3}$ in the particle phase because of its low volatility. Depending on the region, even more iSOA is formed by LISOPOOHOOH than LIEPOX, like over the Middle East. Indeed, the sum of LIEPOX and LISOPOOHOOH mass concentration comprises up to 90 % of the iSOA mass.

IGLYOXAL (Fig. 3e, f) and the sum of the other partitioning iSOA precursors (panels g, h) show similar global distributions and concentrations. Nevertheless, reactive uptake is more efficient in producing more IGLYOXAL SOA (panel f) than the other partitioning iSOA precursors (panel h). IGLYOXAL shows similar maxima as LIEPOX over the American continent, north of Myanmar and over Siberia. The sum of other partitioning iSOA precursors shares areas of peak values with LISOPOOHOOH, pointing out the different iSOA formation processes. Similarly, up to 8 % of iSOA is formed by IGLOYXAL, and the remaining 2 % mainly consists of C59OOH.

Particle concentrations seem high taking into account that possible isoprene IVOCs and more volatile SVOCs were excluded. Hodzic et al. (2016) hypothesize that modeled SOA concentrations might compare better to observed SOA levels, if a faster turnover was simulated. This includes stronger
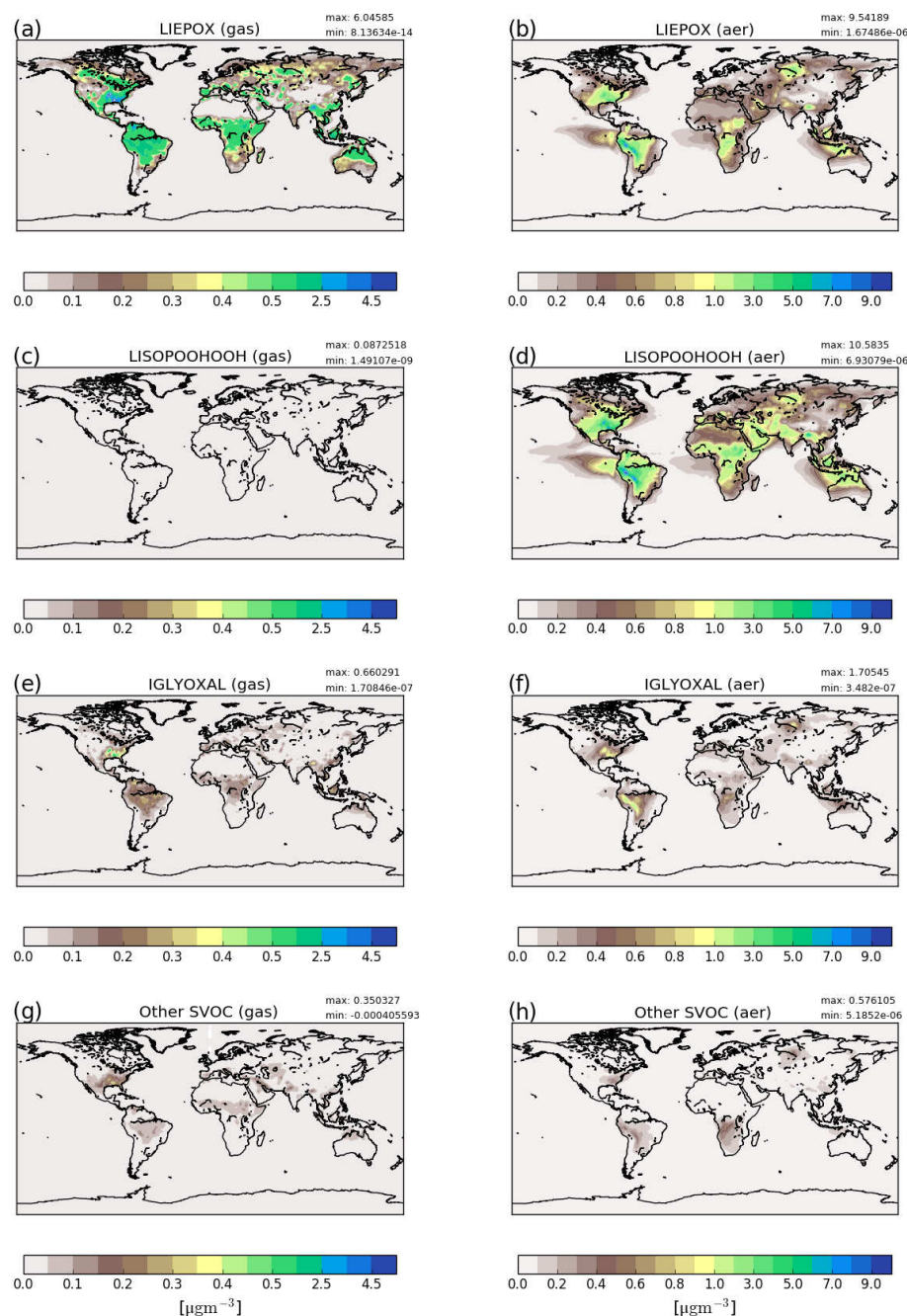
**Figure 3.** Reference run average surface distribution of precursor gases (**a, c, e, g**) and corresponding component concentration in the particle phase (**b, d, f, h**) in µg m$^{-3}$ for June, July and August 2012. Since concentrations of non-LISPOOHOOH iSOA are below 1 µg m$^{-3}$, they are shown together in (**g**) and (**h**). Different scales are used for precursors and iSOA to capture the concentration ranges accordingly. Note that the concentration scales are not linear and focus on low concentrations.

SOA formation, but also stronger removal. Currently, global models usually account for deposition loss, but ignore removal processes as fragmentation, aqueous-phase reactions and in-particle photolysis. The next section (Sect. 3.1.2) compares iSOA production to SOA production in AeroCom and explains the high concentrations described here. Including more aerosol sinks following Hodzic et al. (2016) could

reduce these concentrations even if iSOA production remains as it is currently simulated (see Sect. 3.2.5).

To summarize, Fig. 3 shows that particle formation not only depends on precursor concentrations, but also on available preexisting aerosol. Since all compounds are produced by isoprene the global distribution of the individual gases does not differ a lot. In contrast to the annual mean, the north-

**Table 3.** Total annual chemical production of individual iSOA precursors in 2012 and the corresponding amount of iSOA formed. In parentheses the corresponding yields are given; for the gas phase this includes how much of the total isoprene was converted to precursors and the yield of those precursors into iSOA for the global annual budget.

| Species | Gas-phase production in Tg C (fraction of isoprene source) | Particle formation in Tg C (individual yield in %) |
|---|---|---|
| LIEPOX | 94.0 (24 %) | 21.0 (22 %) |
| IGLYOXAL | 19.8 (5 %) | 3.6 (20 %) |
| LISOPOOHOOH | 35.1 (9 %) | 27.9 (79 %) |
| C59OOH | 6.5 (2 %) | 2.8 (43 %) |
| LC578OOH | 4.5 (1 %) | 0.3 (15 %) |
| LNISOOH | 0.5 (0.1 %) | 0.1 (20 %) |

ern Australian maximum does not appear that prominently during the northern hemispheric summer. Hence, the great impact in the northeastern US is clearly visible. For Europe, even during summer, iSOA seems to play a minor role compared to the equatorial regions due to prevalent vegetation (Steinbrecher et al., 2009).

### 3.1.2 Global iSOA budget

The global annual budget for isoprene-derived secondary organic aerosol is shown in Fig. 4. For the evaluated simulation period of 2012 a total of 392.1 Tg C isoprene was emitted, which is a bit lower than the range of estimated isoprene emissions of 440–660 Tg C (Guenther et al., 2006; Henrot et al., 2017). The oxidation of isoprene leads to the production of 160.4 Tg C of the six iSOA precursors identified in this study. Comparing it to the initially emitted amount, 41 % of isoprene is chemically transformed into iSOA precursors; 24 % of isoprene ends up as IEPOX, 9 % as LISOPOOHOOH, 5 % as IGLYOXAL, 2 % as C59OOH, 1 % as LC578OOH and 0.1 % as LNISOOH (see Table 3). For LIEPOX 94.0 Tg C is produced, which agrees very well with the 95 ± 45 Tg C estimated by Paulot et al. (2009). Of the total produced iSOA precursors, about a third (56.7 Tg C) forms iSOA. Half of iSOA is formed by reactive uptake, through which IEPOX contributes 21.0 Tg C and glyoxal 3.6 Tg C, corresponding to a reactive uptake yield of 22 % (LIEPOX) and 20 % (IGLYOXAL), respectively. Since the reactive uptake is irreversible and the partitioning species are semi- and low-volatile compounds, evaporation is several orders of magnitude lower than condensation. This results in an annual overall isoprene SOA yield of 15 % and a global burden of 0.6 Tg C. An isoprene SOA yield of 15 % lies in the range of 1 % to 30 % under different conditions observed by Surratt et al. (2010). Sinks of the precursor gases are chemical loss including photolysis and dry and wet deposition. The majority of precursors is destroyed chemically, and the second most important sink is wet deposition. Aerosols can be
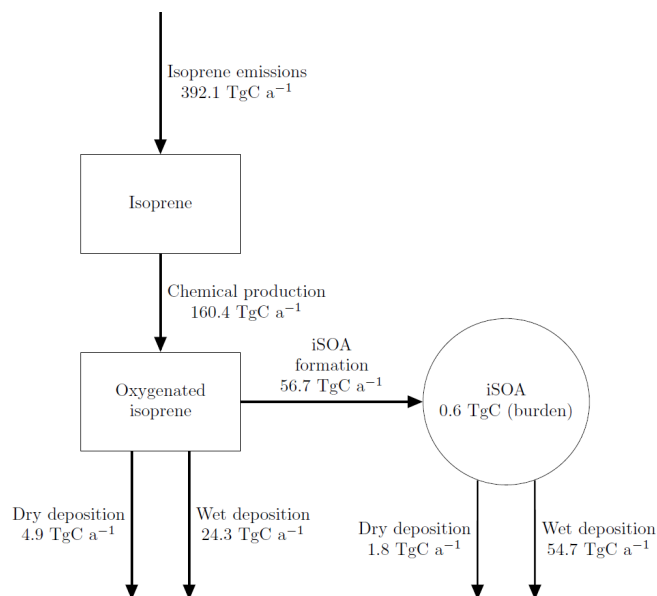


**Figure 4.** Global budgets for isoprene-derived secondary organic aerosol and its precursors (sources and sinks in Tg C a$^{-1}$ and burden in Tg C) predicted by the ECHAM–HAMMOZ reference simulation for 2012. For details about the individual compounds see Table 3.

lost via three processes in ECHAM–HAMMOZ: sedimentation and dry or wet deposition. For iSOA sedimentation is 0.2 Tg C and is for a clearer structure not included in Fig. 4. The main loss of iSOA is wet deposition, removing 54.7 Tg C of the total of 56.7 Tg C.

Table 4 shows the iSOA budget in Tg to be comparable with the mean values from AeroCom (Aerosol Comparisons between Observations and Models) given in Tsigaridis et al. (2014). As can be seen from Table 4, the iSOA production in ECHAM–HAMMOZ in the reference simulation exceeds the total SOA from AeroCom in the upper third quartile limit. Even if this comparison seems to show a vast overestimation by ECHAM–HAMMOZ, 56.7 Tg C iSOA does not reach the lower end of the top-down-estimated source strength ranging from 140–910 Tg C a$^{-1}$ (Goldstein and Galbally, 2007; Hallquist et al., 2009). Therefore, according to these studies, AeroCom generally produces too little SOA, while our new approach might lead to more realistic SOA concentrations. Using the range of 140–910 Tg C a$^{-1}$ for total SOA and our iSOA production of 56.7 Tg C a$^{-1}$ would imply that isoprene contributes between 6 % and 41 % to total SOA. This does not seem unrealistic. Dry deposition and wet deposition are higher than the AeroCom mean value because the iSOA burden is larger. Nevertheless, in ECHAM–HAMMOZ wet deposition is more than 10 times higher than dry deposition, something that is not seen in AeroCom. First, this might point to a too-low aerosol dry deposition in ECHAM–HAMMOZ. Second, high wet deposition might be caused by a moisture and convection overestimation of ECHAM6 in

**Table 4.** Comparison of the ECHAM–HAMMOZ iSOA budget to total SOA budget terms from AeroCom (annual OA budget like in Fig. 1 in Tsigaridis et al., 2014; Kostas Tsigaridis, personal communication, 14 September 2017).

|  | ECHAM–HAMMOZ | AeroCom mean | AeroCom range |
| --- | --- | --- | --- |
| Sources | $138.5\,\mathrm{Tg\,a^{-1}}$ | $36.3\,\mathrm{Tg\,a^{-1}}$ | $12.7–120.8\,\mathrm{Tg\,a^{-1}}$ |
| Dry deposition | $4.4\,\mathrm{Tg\,a^{-1}}$ | $5.7\,\mathrm{Tg\,a^{-1}}$ | $1.4–14.5\,\mathrm{Tg\,a^{-1}}$ |
| Wet deposition | $133.6\,\mathrm{Tg\,a^{-1}}$ | $47.9\,\mathrm{Tg\,a^{-1}}$ | $12.4–113.1\,\mathrm{Tg\,a^{-1}}$ |
| Burden | $1.4\,\mathrm{Tg}$ | $1.0\,\mathrm{Tg}$ | $0.3–2.3\,\mathrm{Tg}$ |
| Lifetime | 3.7 days | 8.2 days | 2.4–14.8 days |

the tropical regions where most iSOA is formed. Finally, the iSOA burden in ECHAM–HAMMOZ is also higher than the mean of AeroCom, while an iSOA lifetime of 3.7 days is in the lower end. The comparably short lifetime of 3.7 days is mainly caused by the quick wet deposition loss of iSOA. In ECHAM–HAMMOZ, iSOA is produced in tropical regions with high relative humidity and active convection, which trigger the wet deposition loss of particle-phase iSOA near the source regions.

As stated in Hodzic et al. (2016), global models are missing aerosol sinks, like in-particle fragmentation and particle photolysis, and should therefore overestimate SOA formation. On the contrary, global models tend to underestimate SOA formation. The comparison of ECHAM–HAMMOZ iSOA to the total SOA of other models shows that the criticized underestimation is more than resolved, since no SOA from aromatics or terpenes is considered in this study. Including semi-explicit chemistry and explicit partitioning leads in ECHAM–HAMMOZ to a high isoprene SOA yield, which motivated several sensitivity runs.

### 3.2 Sensitivity runs

#### 3.2.1 Comparison to pseudo-chemistry SOA

In order to compare the differences in the atmospheric iSOA loads when using the novel coupling of SALSA and MOZ with detailed iSOA chemistry (see Sect. 2.1.3) or when using a more parameterized VBS approach, an ECHAM–HAM simulation that applies VBS (RefVBS) for iSOA formation was run. All input parameters in RefBase and RefVBS are the same, and the climate model ECHAM6 is exactly the same version. However, the major difference is the calculation of atmospheric chemistry. ECHAM–HAM, when it is not coupled to MOZ, uses parameterizations for sulfate aerosol formation and reads in offline fields for oxidant concentrations, while HAM in ECHAM–HAMMOZ obtains chemical information from MOZ. Furthermore, the SOA precursor formation approaches differ. As explained in Sect. 2.1.2 ECHAM–HAM with SALSA uses fixed yields to form SOA precursors from oxidation reactions. Thus, differences in iSOA precursors and iSOA concentrations are caused by differences in the level of sophistication in solving the atmospheric chemistry. Furthermore, the volatilities

of the SOA precursors in the two models differ, which will be discussed in more detail below.

To compare the semi-explicit chemistry and explicit compound-wise partitioning to the pseudo-chemistry and VBS system, an ECHAM–HAM run was performed just including isoprene emissions to form only iSOA in both models. From these isoprene emissions ECHAM–HAM produces gas-phase compounds of the VBS classes VBS0 and VBS1. In these simulations the yield for nonvolatile SOA precursors is set to zero and thus no VBSnonvol is formed from isoprene. VBS0 and VBS1 refer to compounds with $\log 10(C^*) = 0$ and $\log 10(C^*) = 1$ ($C^*$ in $\mathrm{\mu g\,m^3}$), respectively. VBS0 and VBS1 are classes containing SVOCs comparable to ECHAM–HAMMOZ C59OOH, LC578OOH and LNISOOH. Additionally, ECHAM–HAMMOZ includes the compound LISOPOOHOOH, which would be attributed to the class VBSnonvol, but as mentioned above, such a low-volatile compound is not produced from isoprene in the ECHAM–HAM with VBS. Further, ECHAM–HAM does not include IEPOX and glyoxal SOA, and thus these two compounds are not included in this comparison, although they contribute to iSOA in RefBase. The differences between the chemical production of SOA precursors in ECHAM–HAMMOZ and ECHAM–HAM lead to differences in the amount of compounds of different volatilities. ECHAM–HAMMOZ chemistry yields very high amounts of LISOPOOHOOH and less of other SVOCs. In contrast, the pseudo-chemistry in ECHAM–HAM with VBS only leads to the formation of SVOCs from isoprene chemistry, lacking the compounds of lowest volatility. Total iSOA formed by partitioning including SVOCs from ECHAM–HAM RefVBS is compared to iSOA from SVOCs and LVOCs in the ECHAM–HAMMOZ reference run RefBase.

The formed precursors in the gas phase from RefVBS compared to the precursors from RefBase are shown in Fig. 5. From the higher gas-phase concentrations (Fig. 5b), it can be seen that the VBS system only includes semi-volatile compounds. The emission pattern of MEGAN is clearly visible in both model results, but in RefBase some isoprene-emitting areas are hard to distinguish because the concentrations are very low.

Nevertheless, the low gas-phase concentrations in RefBase do not mean that fewer iSOA precursors were formed. On
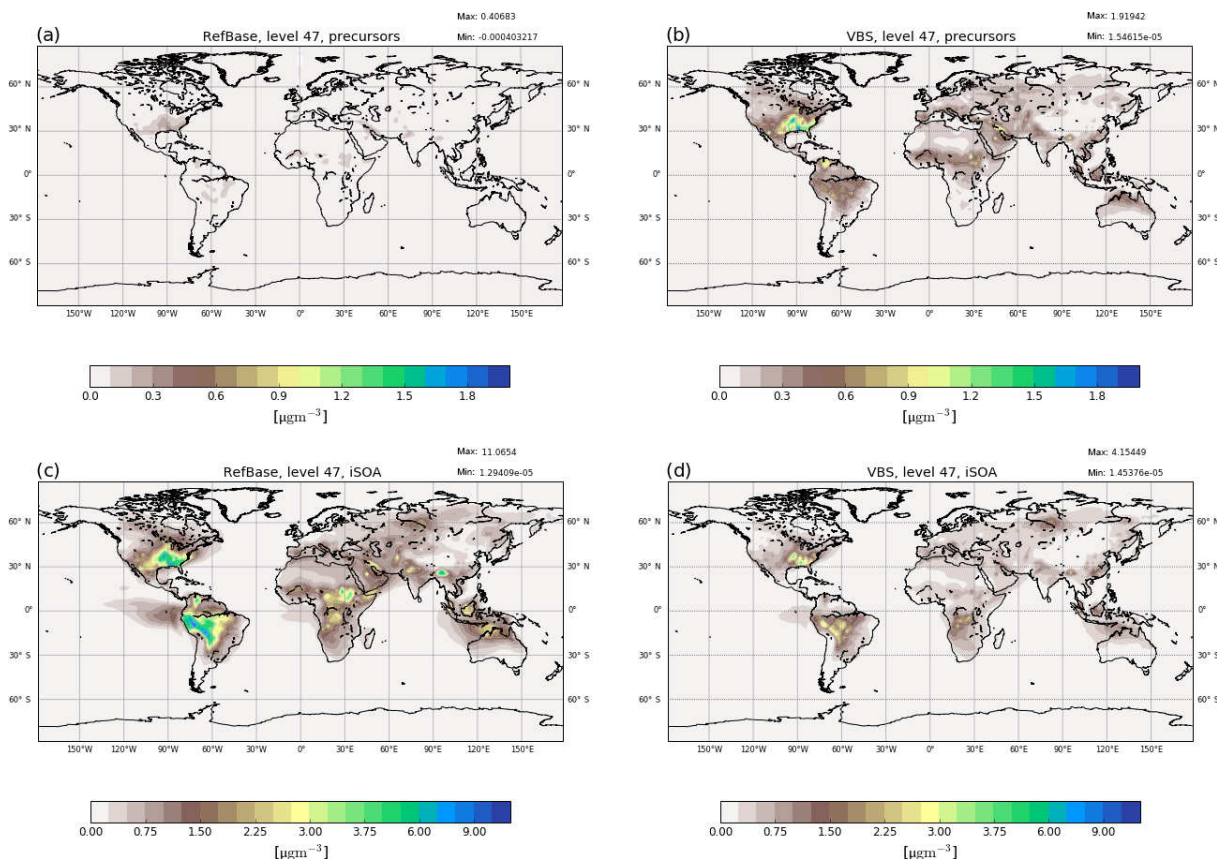
**Figure 5.** Surface average concentrations of gas-phase iSOA precursors **(a, b)** and aerosol-phase iSOA **(c, d)** for June, July and August 2012. Panels **(a)** and **(c)** show concentrations simulated by the reference run RefBase and panels **(b)** and **(d)** show the concentrations calculated by RefVBS using pseudo-chemistry and the VBS system. For RefBase the precursors consist of the four iSOA precursors (LNISOOH, LC578OOH, C59OOH, LISOPOOHOOH) described above; for RefVBS concentrations the sum of the gas-phase VBS classes VBSnonvol, VBS0 and VBS1 is shown.

the contrary, as can be seen in Fig. 5, iSOA from SVOCs and LVOCs in RefBase is overall higher and horizontally transported further than iSOA in RefVBS. Local maxima match between both models, and the higher values in the southeastern US and in the Amazon are captured by both models. However, in the southeastern US RefBase simulates values around $6\,\mu g\,m^{-3}$ over a broader area than RefVBS, reaching $3.5\,\mu g\,m^{-3}$ in two more local maxima. Similarly, over the Amazon and north of the Andes RefBase simulates up to $9\,\mu g\,m^{-3}$, while RefVBS reaches $3\,\mu g\,m^{-3}$. Both simulations also agree on a local maximum in Central Africa and over northern Australia and Indonesia. Again, peak concentrations differ, here by a factor of around 2.

RefVBS includes more SVOCs than RefBase, leading to an equilibrium in RefVBS between gas-phase and aerosol-phase iSOA, which favors higher gas-phase concentrations than seen in RefBase. This results from different chemical precursor formation, with the semi-explicit MOZ forming on average lower-volatile SOA precursors that favor partitioning to the particle phase. LISOPOOHOOH formation is not taken into account in the ECHAM–HAM pseudo-chemistry

formulation, which only forms SVOCs and explains the comparably low iSOA yields. Additionally, LIEPOX SOA and IGLYOXAL SOA, which are not shown in Fig. 5 but are included in RefBase, lead to increased SOA mass in RefBase compared to RefVBS. Increased aerosol mass increases the SOA yield. This could be another reason why more organic mass partitions in the particle phase in RefBase than in RefVBS.

To summarize, given the same isoprene emissions, the ECHAM–HAM pseudo-chemistry produces fewer iSOA precursors with an average higher volatility compared to the semi-explicit chemistry in MOZ, which results in a higher overall iSOA yield in ECHAM–HAMMOZ. Moreover, ECHAM–HAM does not include IEPOX and glyoxal SOA, which may positively affect the gas-to-particle partitioning of the volatile SOA species. This explains the higher precursor concentrations and the lower iSOA concentrations in ECHAM–HAM compared to ECHAM–HAMMOZ. In order to get similar iSOA and precursor concentrations, ECHAM–HAM pseudo-chemistry could be adjusted accordingly.
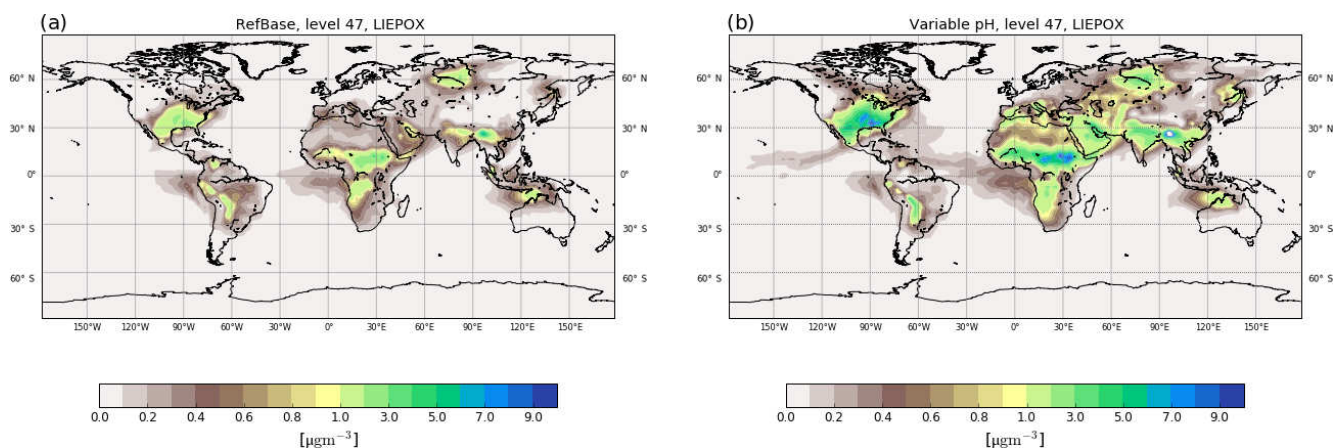
**Figure 6.** Surface average aerosol concentrations in $\mu g\,m^{-3}$ for LIEPOX-derived iSOA with uniform pH value used in the reference run **(a)** and with variable pH value calculated with the AIM aerosol thermodynamics model (see Sect. 2.2) in the sensitivity run $\gamma pH$ **(b)** for the time period of June, July and August 2012.

### 3.2.2 IEPOX sensitivity to aerosol pH

As discussed in Sect. 2.1.1, several laboratory and field studies suggested a pH value influence on the reactive uptake of IEPOX. ECHAM–HAMMOZ does not include ammonium and nitrate aerosol, and therefore no aerosol pH value can be obtained by the model system. As described in Sect. 2.2 a simulation with the AIM aerosol thermodynamics model was performed to obtain the global aerosol pH distribution consistent with ECHAM–HAMMOZ aerosols (Fig. S1). Aerosol pH distribution by AIM is used as input in the sensitivity simulation $\gamma pH$, while the reference simulation Ref-Base uses a uniform value for the reactive uptake coefficient $\gamma$ corresponding to a pH of around 2.5. The simulation $\gamma pH$ was designed to explore the impact of such a dependence. Therefore, based on reaction probability values given in Eddingsaas et al. (2010) and Gaston et al. (2014) a simple function for $\gamma_{IEPOX}$ was formulated and implemented in ECHAM–HAMMOZ:

$$\gamma(pH) = \begin{cases} 10^{-2}, & pH < 2; \\ 0.1[H^+] + 10^{-4}, & pH \in [2, 5]; \\ 0, & pH > 5, \end{cases} \quad (2)$$

where $[H^+]$ is the concentration of protons $H^+$ in the aerosol given in $mol\,L^{-1}$. The reaction probability varies linearly between particles of pH values between 2 and 5. For acidic particles the upper limit of $10^{-2}$ is fixed. For particles that are not acidic enough (pH > 5) no reaction is assumed. The pH distribution (Fig. S1) was then used as model input values. The pH value of the surface aerosols was applied to each model layer, but largest effect can be observed where acidic aerosol and LIEPOX are present.

Figure 6 shows the resulting global surface distribution of $\gamma pH$ run for northern hemispheric summer compared to Ref-Base. Enhancement of reactive uptake in $\gamma pH$ over land is clearly visible; over the southeastern US maximum values

are more than doubled. Further, more areas with $3–4\,\mu g\,m^{-3}$ over Africa, the Middle East and Eurasia can be found where RefBase has values lower than $1\,\mu g\,m^{-3}$. In contrast, suppression of LIEPOX reactive uptake is observable over the Amazon.

Total LIEPOX aerosol produced during this time period increased by 58 % in $\gamma pH$ compared to RefBase. In RefBase an aerosol pH around 2.5 was assumed for all aerosols, also for those that might be less acidic like sea salt aerosol. Nevertheless, compared to $\gamma pH$ less LIEPOX SOA was formed. In $\gamma pH$ most areas are covered by less acidic aerosol, but LIEPOX is produced or transported to regions where acidic aerosol can be found; this leads to the observed increase in iSOA formation.

As an alternative explanation for the pH value dependence, Xu et al. (2015) hypothesize that IEPOX uptake enhancement could be triggered by sulfate aerosol. Although sulfate aerosol is simulated, no sensitivity study was performed here due to lack of process understanding and possible reactive uptake parameterizations.

### 3.2.3 Sensitivity to evaporation enthalpy

Tsigaridis and Kanakidou (2003) point out the sensitivity of SOA formation to the evaporation enthalpy $\Delta H_{vap}$. Nevertheless, due to the lack of knowledge of $\Delta H_{vap}$ for the different organic compounds, usually a fixed value or a rather low value is used for all of them (Epstein et al., 2009). Depending on the study, different estimations for $\Delta H_{vap}$ were made, ranging between 30 and $156\,kJ\,mol^{-1}$ (Athanasopoulou et al., 2012). Farina et al. (2010) also use the Clausius–Clapeyron equation to calculate saturation concentrations for a variety of organics using $30\,kJ\,mol^{-1}$ as the $\Delta H_{vap}$. To explore the impact of this assumption and the impact of a lower evaporation enthalpy, the sensitivity run
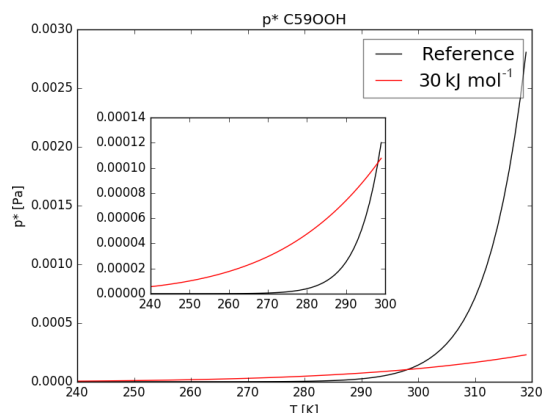
**Figure 7.** Curves given by the Clausius–Clapeyron equation (Eq. 1) for C59OOH. The red curve is obtained by setting $\Delta H_{\text{vap}} = 30\,\text{kJ}\,\text{mol}^{-1}$, and the black one describes the parameters used in the reference run (see Table 1).

$\Delta H_{30}$ was designed to use $\Delta H_{\text{vap}} = 30\,\text{kJ}\,\text{mol}^{-1}$ but keep the same reference saturation vapor pressure (see Table 1).

As an example Fig. 7 shows the curves given by Eq. (1) using $\Delta H_{\text{vap}}$ of the reference run and the sensitivity run. Equation (1) changes its curve form drastically when lowering $\Delta H_{\text{vap}}$ from values around 150 to $30\,\text{kJ}\,\text{mol}^{-1}$. For temperatures lower than the reference value of 298.15 K the saturation vapor pressure of $\Delta H_{30}$ $p^*_{\Delta H_{30}}$ is higher compared to the reference $p^*$, but for temperatures higher 298.15 K the opposite is the case (see Fig. 7).

As a result, the impact of variable $\Delta H_{\text{vap}}$ on iSOA formation varies with temperature and therefore also with region and height. The sensitivity simulation $\Delta H_{30}$ ran for June, July and August 2012 with changed Clausius–Clapeyron equation curves according to Fig. 7. Even during this northern hemispheric summer, from a global perspective the atmosphere is on average cooler than 298.15 K, especially at higher altitudes. Therefore, global total iSOA production in $\Delta H_{30}$ for the considered time period is just 0.6 Tg C lower compared to RefBase. This is a reduction of 4 % of the total amount produced in RefBase in June, July and August 2012. For surface temperatures higher than 298.15 K, $p^*_{\Delta H_{30}}$ is orders of magnitude lower than the reference $p^*$, but gas-phase concentrations of iSOA precursors are high enough that no significant impact on iSOA concentrations is seen. In agreement, surface concentration fields do not change much and are therefore not shown.

The assumption made by Farina et al. (2010) connected with the estimation of $p^*_0$ of iSOA precursors in this study therefore does not lead to significant changes in model results. The lowest sensitivity to $\Delta H_{\text{vap}}$ can be found in the LVOC LISOPOOHOOH. In ECHAM–HAMMOZ sensitivity to $\Delta H_{\text{vap}}$ increases with the volatility of the compounds, and therefore $\Delta H_{\text{vap}}$ should be crucial for additional consid-

eration of SVOCs and IVOCs, which will be added to the model in a future study.

### 3.2.4 Uncertainty estimation saturation vapor pressure

As described in Sect. 2.1.1 the group contribution method by Nannoolal et al. (2008) in combination with the boiling point method by Nannoolal et al. (2004) were used to obtain the saturation vapor pressure of originated isoprene products as a function of temperature. Group contribution methods estimate the contribution of functional groups to saturation vapor pressure. The Nannoolal et al. (2008) group contribution method is based on 68 835 data points of 1663 components and just needs two inputs: the molecular structure and the normal boiling point. Nannoolal et al. (2008) report a good performance against measurements. Nevertheless, when its performance is compared to compounds outside the training set, the results become worse (Barley and McFiggans, 2010; OMeara et al., 2014). Barley and McFiggans (2010) underline the fact that databases are typically biased towards mono-functional groups, and therefore group contribution methods trained with these data perform well for volatile fluids, but not for low-volatility compounds. OMeara et al. (2014) arrive at similar conclusions; they tested seven saturation vapor pressure estimation methods and found that even if the Nannoolal et al. (2008) method results in the lowest mean bias error, the method shows poor accuracy for compounds with low volatility. This tendency also holds true for the other tested methods, showing increasing error with an increasing number of hydrogen bonds. This systematic error results in an SOA formation overestimation.

Since the underlying databases used for group contribution methods, also for Nannoolal et al. (2008), are often biased and do not include complex polyhydroperoxides (Kurten et al., 2016), a sensitivity run with the group contribution method EVAPORATION was performed (EVA). EVAPORATION was designed to include hydroperoxide and peracid molecular structures and does not need a boiling point as an input (Compernolle et al., 2011). Especially for the highly oxidized compound LISOPOOHOOH, this could reduce the model error.

Moreover, McFiggans et al. (2010) analyzed the dependence of SOA formation on the saturation vapor pressure of each compound and state that SOA mass is highly sensitive to this parameter. Up to 30 % overestimation can result from ignoring the nonideality of the organic mixture.

These studies already identified and emphasized several causes and consequences of the various group contribution methods. Thus, $\log_{10} C^*_0$ values from the Nannoolal et al. (2008) method are compared to values obtained by the EVAPORATION method and a simple group method based on oxygen, carbon and nitrate atoms in the molecule described in Donahue et al. (2011) (Table 5).

As can be seen from Table 5, the $\log_{10} C^*_0$ values do not differ much between the simple group contribution method of

**Table 5.** Comparison of logarithmic saturation concentrations $\log_{10} C_0^*$ at 300 K for the iSOA precursors calculated via the group contribution method used in RefBase (Nannoolal et al., 2008), used in EVA (Compernolle et al., 2011) and a simple group contribution method formulated by Donahue et al. (2011). In brackets the $\log_{10} C_0^*$ values for the isomers are shown.

|  | Nannoolal et al. (2008) | Compernolle et al. (2011) | Donahue et al. (2011) |
|---|---|---|---|
| LNISOOH | 1.2 (1.4) | 2.2 (2.8) | 1.3 |
| LISOPOOHOOH | −1.6 (−1.9) | −0.2 (−0.9) | −0.7 |
| LC578OOH | 1.1 (1.1) | 1.7 (1.7) | 1.0 |
| C59OOH | 0.8 | 1.4 | 1.0 |

Donahue et al. (2011) and the one by Nannoolal et al. (2008), except for the lowest-volatility compound LISOPOOHOOH. For LISOPOOHOOH, Nannoolal et al. (2008) predict a much lower volatility than Donahue et al. (2011). This difference agrees with the findings of the studies described above and indicates that LISOPOOHOOH iSOA formation might be too high in ECHAM–HAMMOZ. In contrast, the $\log_{10} C_0^*$ values from the Nannoolal et al. (2008) method strongly differ from the $\log_{10} C_0^*$ calculated by the EVAPORATION method (Compernolle et al., 2011). All compounds are estimated to be more volatile when EVAPORATION is used. This changes the classification, according to the definitions by Donahue et al. (2012), of LISOPOOHOOH, which was referred to as an LVOC and would now be an SVOC ($\log_{10} C_0^* > -0.5$), and LNISOOH, which was called an SVOC and would now be an IVOC (second isomer, $\log_{10} C_0^* > 2.5$).

Also given are the $\log_{10} C_0^*$ values for the different isomers. The Nannoolal et al. (2008) method and EVAPORATION method agree well on the volatility of the isomers. Both calculate that the second LNISOOH isomer is more volatile, the second LISOPOOHOOH isomer is less volatile and that there is no difference between the LC578OOH isomers. Due to computational resource limits, no further sensitivity runs using the isomers instead were done. Nevertheless, from the $\log_{10} C_0^*$ values and the values in Table 1, it is clear that for LC578OOH there is no difference caused by isomeric structures in volatility. For LNISOOH the other isomer is even slightly more volatile and for LISOPOOHOOH the opposite holds true; its second isomer is slightly less volatile. Since LNISOOH is only formed in very low concentrations these deviations might not be visible in iSOA formation.

The large differences between the Nannoolal et al. (2008) method and EVAPORATION method motivated the sensitivity run EVA, which was performed for 1 year to evaluate the iSOA budget. The higher volatility of iSOA precursors in EVA leads to less surface area available for reactive uptake of LIEPOX and IGLYOXAL. The changes in the production rates and iSOA burden can be found in Table 6 (Stadtler, 2018). Total iSOA production is reduced by 12.8 % and the iSOA burden by 16.7 %. This reduction is mainly explained by reduction in LISOPOOHOOH SOA and LIEPOX SOA formation, although LC578OOH SOA and

**Table 6.** Percentage changes in total iSOA formation in 2012 for the sensitivity run EVA using EVAPORATION instead of Nannoolal et al. (2008) to estimate the saturation vapor pressure and the evaporation enthalpy of the isoprene-derived SOA precursors.

| Change in EVA compared to RefBase | | |
|---|---|---|
|  | % | Tg C |
| LIEPOX | −5.2 | −1.1 |
| IGLYOXAL | −5.2 | −0.2 |
| LISOPOOHOOH | −16.7 | −4.6 |
| C59OOH | −36.3 | −0.1 |
| LC578OOH | −50.0 | −0.3 |
| LNISOOH | −90.0 | −0.1 |
| Total iSOA | −12.8 | −7.3 |
| Total iSOA burden | −16.7 | −0.1 |

LNISOOH SOA production is reduced by 50 % and 90 %. It should be noted that in EVA, most iSOA is also produced by LISOPOOHOOH with a total of 23.2 Tg C, followed by 20.4 Tg C by LIEPOX in 2012. Therefore, the iSOA composition is still dominated by these two compounds. Surface iSOA concentrations change marginally, and the same patterns are visible as in RefBase and are therefore not shown. Thus, the main conclusions of this study using the reference run RefBase do not change although iSOA production is reduced when using the EVAPORATION method (Stadtler, 2018).

### 3.2.5 Uncertainty in LISOPOOHOOH aerosol

Section 3.1.1 and 3.1.2 showed the large impact of LISOPOOHOOH on iSOA in ECHAM–HAMMOZ, but as seen in Sect. 3.2.4, the uncertainty in LISOPOOHOOH vapor pressure is high. The large contribution to iSOA remains, regardless of whether the Nannoolal et al. (2008) or EVAPORATION (Compernolle et al., 2011) method is used for saturation vapor pressure estimation. While it is difficult to conceive additional sources of LISOPOOHOOH, there are two pathways through which the impact of LISOPOOHOOH on particle-phase concentrations could be lower than estimated here: (1) reduction of chemical LISOPOOHOOH production

in the gas phase and (2) introduction of additional SOA sinks, e.g., in-particle decay and particle photolysis.

As pointed out in Sect. 2.1.1, the direct LISOPOOHOOH precursor (LISOPOOHO2) 1,5-H shift reaction is missing in the JAM3 chemical mechanism. To test the impact of this reaction, which leads to different iSOA precursors than LISOPOOHOOH, a simplified pseudo-reaction was added to the mechanism in the sensitivity experiments HshiftLIE and HshiftC5 (Sect. 2.2). Both include the isomerization reaction of LISOPOOHO2, but yield different iSOA precursors. In HshiftLIE the LISOPOOHO2 1,5-H shift produced LIEPOX, while in HshiftLC5 LC578OOH is produced instead. The real impact of the 1,5-H shift might lie between these runs, but they agree well with respect to the impact on total iSOA. Both runs diagnose a reduction in chemical LISOPOOHOOH production by 95 % and a reduction in LISOPOOHOOH SOA formation by 92 %. Nevertheless, either LIEPOX SOA or LC578OOH SOA formation increases due to the increased gas-phase production of these compounds in each run. IEPOX SOA in HshiftLIE increases by 31 %, while there is 13 times more LC578OOH SOA in HshiftLC5. Therefore, the iSOA burden is reduced in HshiftLIE by 37 % and in HshiftLC5 by 28 %. Global distributions for the simulated time period can be found in Supplement S2, Figs. S2 and S3.

Concerning the potentially important additional iSOA sink processes, we tested particle decay with a simple parameterization using a half-life of 4 h following D'Ambro et al. (2017a) (DECAY). Hodzic et al. (2015) claim that SOA photolysis might be as high as $J_{SOA} = 0.04 \% \, J_{NO_2}$ and would thus constitute an efficient sink, which could lead to a substantial reduction of SOA mass in the atmosphere. Malecha and Nizkorodov (2016) criticize this photolysis rate as being too high. Following the simple scaling approach of Hodzic et al. (2015), we implemented iSOA photolysis with a rate of $J_{iSOA} = 0.004 \% \, J_{NO_2}$ and tested the impact of this reaction in simulation JPHOT (Stadtler, 2018). Including both processes leads to a reduction of the iSOA burden by 50 %, whereby LISOPOOHOOH is reduced most effectively.

We conclude that there are indeed processes that have the potential to substantially reduce the contribution of LISOPOOHOOH to SOA formation and thus lower the iSOA burden compared to our base simulation by up to 50 %. However, quantification of the rates of these processes remains highly uncertain. Therefore they were not included in the base version of our chemical mechanism.

### 3.3 Comparison with observations

In order to evaluate how much total organic aerosol (OA), including primary and secondary organic aerosol, is related to iSOA, iSOA concentrations and O : C ratios from ECHAM–HAMMOZ are compared to atmospheric mass spectrometry (AMS) measurements from the different field campaigns given in Table 7. Measurements were selected from the AMS
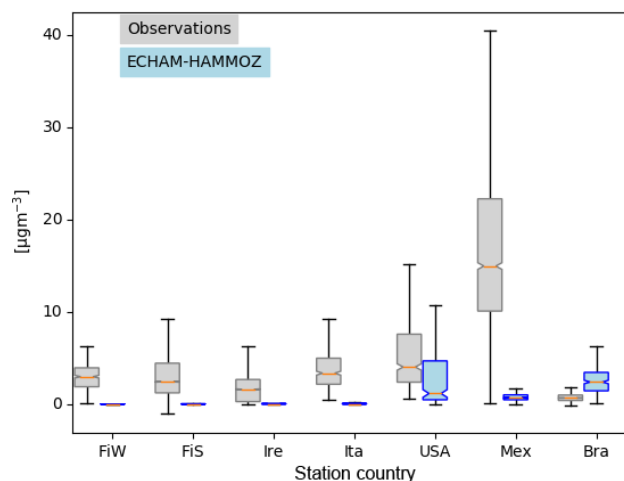


**Figure 8.** Box plots showing the variability of concentrations measured and the corresponding instantaneous values from ECHAM–HAMMOZ. Countries of measurement campaigns are given. The abbreviations refer to the following. FiW: Helsinki, Finland (Winter), FiS: Helsinki, Finland (Spring), Ire: Mace Head, Ireland, Ita: Po Valley, Italy, USA: Houston Texas, USA, Mex: Mexico City, Mexico, Bra: Manaus, Brazil. The model time resolution is 3 h; all values given from the observations are included, meaning that they have a higher time resolution.

global database (Zhang et al., 2017) according to the availability of elemental ratios. All campaigns took place either in Europe or North America and include six different countries. In Helsinki, Finland, winter and spring measurements are available.

Figure 8 shows the quartiles of the time series of the concentrations in the different locations. The European data sets display a variety of local OA sources. For Helsinki, Carbone et al. (2014) report a variety of local sources for OA including biomass burning, traffic, coffee roasting and SOA from long-range transport. In Mace Head two different OA types are measured depending on the advection of either marine air or continental air (Dall'Osto et al., 2010). Saarikoski et al. (2012) identified in the Po Valley a complex mixture of OA with local and regional sources, mainly from anthropogenic origin. For Finland, Ireland and Italy, ECHAM–HAMMOZ reveals a minor contribution of iSOA to OA; this can be explained by the measurement time periods in winter or early spring when vegetation in Europe does not emit large isoprene amounts (Steinbrecher et al., 2009).

Looking at the concentrations measured in Houston, Texas, USA, it can be seen that a large part of the variability is captured by iSOA, which is explained by high isoprene emissions found in the southeastern US. ECHAM–HAMMOZ median and percentiles are still lower than the observations since the observations include total OA. The organic aerosol in Mexico City was measured at an urban super-site and covers such a big range of concentrations, which are dominated by anthropogenic emissions in-

**Table 7.** Overview of ambient measurement locations, time periods and references. For Helsinki there are two time series, one during winter (W) and the second during spring (S).

| Location | Observation time period | Reference |
| --- | --- | --- |
| Helsinki, Finland (60.2° N, 24.95° E) | 8 Jan–14 Mar 2009 (W) | Carbone et al. (2014) |
| | 9 Apr–8 May 2009 (S) | Timonen et al. (2010) |
| Mace Head, Ireland (53.33° N, 9.99° W) | 25 Feb–26 Mar 2009 | Dall'Osto et al. (2010) |
| Po Valley, Italy (44.65° N, 11.62° E) | 31 Mar–20 Apr 2008 | Saarikoski et al. (2012) |
| Houston, USA (29.8° N, 95.4° W) | 15 Aug–15 Sep 2000 | Zhang et al. (2007) |
| Mexico City, Mexico (19.48° N, 99.15° W) | 10 Mar–30 Mar 2006 | Aiken et al. (2009, 2010) |
| Manaus, Brazil (2.58° S, 60.2° W) | 6 Feb–13 Mar 2008 | Chen et al. (2009); Pöschl et al. (2010); |
| | | Martin et al. (2010) |
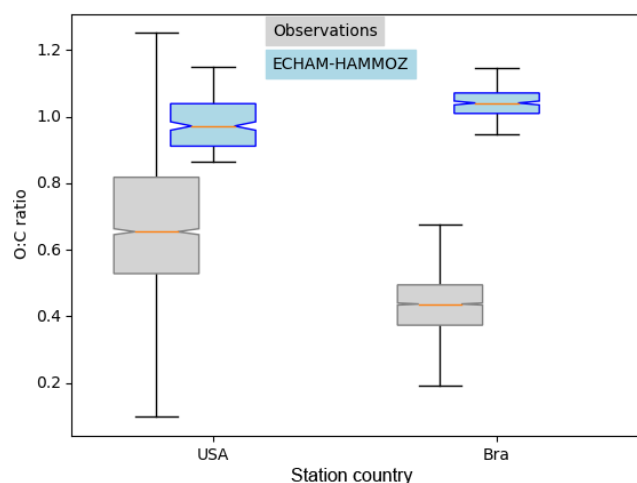


**Figure 9.** Similar to Fig. 8 showing the corresponding O : C ratios of the subset Houston, Texas, USA, and Manaus, Brazil. The O : C ratios shown here are corrected by the factor 1.27 according to Canagaratna et al. (2015).

cluding biomass burning, nitrogen-containing OA and primary hydrocarbon, like OA associated with traffic (Aiken et al., 2009). According to the concentrations simulated by ECHAM–HAMMOZ, just a minor part of these can be explained by iSOA. Manaus, Brazil, is located in the Amazon Basin and classified as a pristine environment close to preindustrial conditions (Pöschl et al., 2010; Martin et al., 2010). Therefore, the particles are nearly purely biogenic and Martin et al. (2010) report an upper limit of 5 % primary organic aerosol. These conditions are ideal to compare them to ECHAM–HAMMOZ just including iSOA because isoprene emissions are high in the Amazon Basin and should dominate the OA there. As can be seen in Fig. 8, HAMMOZ simulates overall higher iSOA concentrations than the OA concentrations measured. Moreover, higher peak values are simulated and the median is higher than the upper 1.5 interquartile range whisker of observed concentrations.

For Houston, Texas and Manaus, the comparison of the concentrations simulated by ECHAM–HAMMOZ and the concentrations measured by AMS shows that ECHAM–HAMMOZ relates a large part of the observed OA to iSOA. Since iSOA seems to play a role in these regions, O : C ratios are compared as well. Due to restricted iSOA formation in ECHAM–HAMMOZ only from six iSOA precursors, which are highly oxidized molecules with molecular O : C ratios between 0.6 and 1.4, the modeled O : C ratio just covers small variability and is around 1 in both regions; see Fig. 9.

The comparison of the concentration spectrum in Houston, Texas, showed a large part to be attributed to iSOA; this modeled subset covers upper values of the O : C ratio between 0.8 and 1.1, which still lie within the 75th percentile and the upper $1.5 \times$ IQR whisker of the measured data. This is related to missing SVOCs and IVOCs usually having lower O : C ratios and the contribution of POA to OA, which is not included in this comparison because no assumptions of POA O : C ratios are made.

In contrast, the OA measured in Manaus located in the Amazon Basin, which consists of 95 % SOA, does not show as high O : C ratios as iSOA modeled by ECHAM–HAMMOZ. The median of observed aerosol lies at 0.4 instead of 1. Certainly part of it is explained by missing SVOCs and IVOCs in ECHAM–HAMMOZ, but it might also be related to SOA from organic molecules other than isoprene.

For Manaus an overestimation of iSOA concentrations by the model might be related to mistakes in emissions and in the chemical mechanism, missing sink processes and uncertainties in $p^*$. In terms of the O : C ratio of modeled iSOA between 0.6 and 1.4, the simulated values are covered by the ambient values in Houston, Texas, but not in Manaus. This points to SVOCs, IVOCs and SOA from sources other than isoprene.

To summarize, isoprene emissions do not dominate OA in Europe, and therefore the model shows iSOA having a small contribution to concentrations there. In contrast, OA in the Americas is more impacted by iSOA, especially in the USA and Brazil.

## 4 Discussion

The comparison of RefBase to AeroCom, ECHAM–HAM and AMS measurements in the isoprene-dominated area of Manaus in the Amazon Basin revealed that semi-explicit treatment of atmospheric chemistry, at least for isoprene, leads to much larger SOA production rates and eliminates the low biases found in most other global model studies. In fact, especially over Brazil, SOA now has a tendency to be overestimated. Extrapolating the iSOA production rate to the production rate of SOA in ECHAM–HAMMOZ including SVOCs and IVOCs not only from isoprene, but also from terpenes and aromatics, we expect to find a portion of SOA that cannot be reduced by only including the missing aerosol sinks. Various reasons for this part of the overestimation of iSOA in ECHAM–HAMMOZ could be identified by analyzing the results of the simulations presented in this study and are discussed in the following.

First, overestimation of iSOA may be related to errors in the group contribution method used to estimate the saturation vapor pressure and evaporation enthalpy of iSOA precursors. As discussed in OMeara et al. (2014) and Barley and McFiggans (2010), the Nannoolal et al. (2008) method is problematic in the low-volatility range, giving too-low saturation pressures, which leads to an overestimation of SOA formation. Comparing the logarithm of the saturation concentration at a reference temperature ($\log_{10} C_0^*$) obtained by Nannoolal et al. (2008) to the one using the EVAPORATION (Compernolle et al., 2011) method and to the simple method of Donahue et al. (2011) reveals the largest differences in the lowest-volatile compound LISOPOOHOOH. To assess the impact of a reduced $\log_{10} C_0^*$, a sensitivity simulation using the EVAPORATION method was performed. This simulation showed a reduction in the global annual average iSOA burden of 16.7 %, which is mainly due to reductions in LISOPOOHOOH SOA. Nevertheless, the main conclusions obtained from the reference run are not changed by this sensitivity simulation.

A second aspect leading to a potential overestimation of iSOA is the semi-explicit chemistry itself. Different chemical pathways lead to the formation of isoprene SVOCs and LVOCs, some requiring NO and $NO_3$ for the initial steps followed by OH, $HO_2$ or $RO_2$. The formation of iSOA precursors via $NO_x$-dependent pathways hardly happens, as can be seen in the chemical budget terms. LNISOOH and LC578OOH are formed in very low concentrations and C59OOH might just result from the $HO_2$-dominated pathway. From the chemical branching it can clearly be seen that on average in JAM3 the OH-initiated pathway is preferred, even in regions where NO mixing ratios are higher than 200 pptv (not shown); 90 % of iSOA consists of products from this pathway, mostly IEPOX and LISOPOOHOOH. Highly acidic aerosol is expected in regions where sulfate pollution is high and these regions usually coincide with high $NO_x$, which should suppress LIEPOX forma-

tion. For LIEPOX this might lead to a large overestimation when acidic enhancement is considered. The JAM3 chemical mechanism simulates LIEPOX and LISOPOOHOOH suppression when NO mixing ratios surpass 700 pptv. This feature in the chemistry can only be seen in 3-hourly values of the single grid boxes and vanishes when mean values are evaluated. Once NO mixing ratios are lower, LIEPOX and LISOPOOHOOH are produced again, leading on average to the impression of missing $NO_x$ suppression (Stadtler, 2018). Further, LISPOOHOOH production might be overestimated due to a missing intramolecular 1,5-H shift of LISOPOOHO2 in JAM3, which would lead to products with a saturation vapor pressure around 2 orders of magnitude higher than that of LISPOOHOOH (see Sect. 2.1.1; D'Ambro et al., 2017b). To check the impact on LISOPOOHOOH and the derived iSOA, two tests including the 1,5-H shift of LISOPOOHO2 were evaluated. Gas-phase production of LISOPOOHOOH is reduced by over 90 %, but since the products of the 1,5-H shift still form iSOA, the iSOA burden is only reduced by around 30 %.

Third, the main iSOA formation pathways follow from OH-initiated reactions, which is the main oxidation pathway for isoprene. The ECHAM–HAMMOZ evaluation of Schultz et al. (2018) shows that the tropical region in our model is too wet. This leads to a higher production of OH radicals so that the model atmosphere is more oxidative than the real atmosphere. Tropical regions are where most isoprene is emitted. Thus, gas-phase precursor formation might be overestimated already, which translates into an iSOA overestimation.

Fourth, Kroll et al. (2006) reported that rapid chemical loss of SOA via photolysis could be a possibility to further transform iSOA either to higher oxidized molecules in the particle phase, such as oligomers, or to fragment iSOA compounds, leading to VOC and iSOA reduction. Hodzic et al. (2015) explored the global impact of SOA photolysis and report about a 40 %–60 % mass reduction after 10 days. SOA photolysis is closely related to wet-phase, in-particle chemistry, which is not included in the ECHAM–HAMMOZ chemical mechanism. Thus, simple parameterizations for SOA photolysis and in-particle decay were tested with ECHAM–HAMMOZ, efficiently reducing the iSOA burden by around 50 % due to in-particle decay of LISOPOOHOOH and by around 10 % due to SOA photolysis.

Finally, model limitations in aerosol and cloud processing did not allow us to implement in-cloud iSOA formation. This is not only a potential additional source, but also an additional sink. ECHAM–HAMMOZ just includes wet scavenging based on solubility following Henry's law, but according to Cole-Filipiak et al. (2010) the IEPOX hydrolysis reactions at low pH values have lifetimes comparable to wet deposition. Heterogeneous uptake of IEPOX in cloud droplets and rain would lead to a decrease in gas-phase concentrations, while not resulting in iSOA because it is lost immediately due to precipitation. This would lower iSOA from LIEPOX, which now has a substantial contribution to total iSOA.

## 5  Conclusions

For the first time, the semi-explicit chemical treatment of iso-prene oxidation in the chemical mechanism of a global chemistry climate model was connected to explicit partitioning of individual low-volatility species according to their chemical structures. The chemistry model MOZ includes a total of 779 reactions, of which 147 reactions describe isoprene oxidation. Isoprene oxidation in MOZ leads to iSOA precursors, which are explicitly partitioned and followed in specific aerosol bins by HAM-SALSA. The partitioning is based on the saturation vapor pressure derived from the molecular structure of each single compound. Furthermore, the reactive uptake of isoprene-derived glyoxal and IEPOX was also considered.

These two iSOA formation pathways lead to a global annual average isoprene SOA yield of 15 % relative to the primary oxidation of isoprene by OH, $NO_3$ and ozone in 2012. It was identified that in ECHAM–HAMMOZ most iSOA is produced via the OH-oxidation-initiated pathway, which leads to the production of IEPOX and ISOP(OOH)2, a compound recently detected in experimental studies. Together modeled IEPOX and ISOP(OOH)2 yield a fraction of 90 % of total iSOA mass. In total 56.7 Tg C iSOA is produced. IEPOX forms 21.0 Tg C and ISOP(OOH)2 27.9 Tg C aerosol. 54.7 Tg C iSOA is lost due to wet deposition, which is the main sink for iSOA in ECHAM–HAMMOZ. For 2012 an average iSOA burden of 0.6 Tg C is calculated. These values were compared to SOA budgets in AeroCom. ECHAM–HAMMOZ simulates a higher production rate than all models used in this AeroCom study.

Moreover, this explicit model system enables process understanding and discussion. While exploring the influence of aerosol pH on IEPOX reactive uptake, enhancement of iSOA formation was found, especially over the southeastern US, while suppression could be observed over the Amazon Basin.

Evaporation enthalpy used in previous model studies was compared to the explicitly derived evaporation enthalpy used in ECHAM–HAMMOZ. A huge difference could be found in Clausius–Clapeyron curves, which does not translate to a big impact on iSOA formation due to the fact that only sufficiently low-volatile precursor gases were used.

Changing the volatility of the partitioning precursor gases has a larger impact on iSOA formation and the SOA burden. The group contribution methods by Nannoolal et al. (2008) and Compernolle et al. (2011) were used and annual iSOA formation compared. EVAPORATION estimates higher saturation vapor pressures for all partitioning precursors, leading to a 16.7 % reduction in the global annual average iSOA burden. Nevertheless, the iSOA composition does not change: LISOPOOHOOH and LIEPOX are still the dominant compounds.

LISOPOOHOOH SOA formation can only be reduced by either including new iSOA sinks or the isomerization reaction of the direct LISOPOOHOOH precursor. This 1,5-H shift reaction still leads to iSOA precursors, and thus LISOPOOHOOH SOA is reduced largely by 90 %, but total iSOA burden only by 30 % because the new iSOA precursor still contributes to iSOA.

Comparison of ECHAM–HAMMOZ iSOA concentrations to AMS measurements showed that ECHAM–HAMMOZ does not underestimate iSOA formation. On the contrary, in isoprene-dominated regions like Brazil an iSOA overestimation could be observed, which provides the possibility to explore novel SOA sinks, like in-particle decomposition or photolysis. Not lowering the production rate but including additional sinks is the strategy proposed by Hodzic et al. (2016). They conclude that because several SOA sinks are currently excluded from global models, these models are expected to overestimate SOA concentrations. Instead of the expected overestimation, an underestimation is found in the majority of global models. With our explicit model system connecting the aerosol bin scheme SALSA with the chemistry model MOZ in the framework of the global model ECHAM–HAMMOZ sufficient SOA is produced to explore new sink processes. The simple implementation and quick test of in-particle decay and SOA photolysis reduced the global iSOA burden by about 50 %.

**The Supplement related to this article is available online at https://doi.org/10.5194/gmd-11-3235-2018-supplement.**

*Author contributions.* SS and TK developed the coupling of HAM-SALSA and MOZ. For this TK adjusted the SALSA code to be compatible with MOZ, and accordingly SS worked on the MOZ code to introduce the tracer characteristics (saturation vapor pressure, reactive uptake, etc.) needed by SALSA. The experiments were planned by SS, MS, DT, TK and HK. SS carried out all simulations, including the ECHAM–HAM simulation. SS prepared the paper with contributions from all coauthors.

Edited by: Gerd A. Folberth
Reviewed by: two anonymous referees

# References

Aiken, A. C., Salcedo, D., Cubison, M. J., Huffman, J. A., DeCarlo, P. F., Ulbrich, I. M., Docherty, K. S., Sueper, D., Kimmel, J. R., Worsnop, D. R., Trimborn, A., Northway, M., Stone, E. A., Schauer, J. J., Volkamer, R. M., Fortner, E., de Foy, B., Wang, J., Laskin, A., Shutthanandan, V., Zheng, J., Zhang, R., Gaffney, J., Marley, N. A., Paredes-Miranda, G., Arnott, W. P., Molina, L. T., Sosa, G., and Jimenez, J. L.: Mexico City aerosol analysis during MILAGRO using high resolution aerosol mass spectrometry at the urban supersite (T0) – Part 1: Fine particle composition and organic source apportionment, Atmos. Chem. Phys., 9, 6633–6653, https://doi.org/10.5194/acp-9-6633-2009, 2009.

Aiken, A. C., de Foy, B., Wiedinmyer, C., DeCarlo, P. F., Ulbrich, I. M., Wehrli, M. N., Szidat, S., Prevot, A. S. H., Noda, J., Wacker, L., Volkamer, R., Fortner, E., Wang, J., Laskin, A., Shutthanandan, V., Zheng, J., Zhang, R., Paredes-Miranda, G., Arnott, W. P., Molina, L. T., Sosa, G., Querol, X., and Jimenez, J. L.: Mexico city aerosol analysis during MILAGRO using high resolution aerosol mass spectrometry at the urban supersite (T0) – Part 2: Analysis of the biomass burning contribution and the non-fossil carbon fraction, Atmos. Chem. Phys., 10, 5315–5341, https://doi.org/10.5194/acp-10-5315-2010, 2010.

Athanasopoulou, E., Vogel, H., Vogel, B., Tsimpidi, A. P., Pandis, S. N., Knote, C., and Fountoukis, C.: Modeling the meteorological and chemical effects of secondary organic aerosols during an EUCAARI campaign, Atmos. Chem. Phys., 13, 625–645, https://doi.org/10.5194/acp-13-625-2013, 2013.

Barley, M. H. and McFiggans, G.: The critical assessment of vapour pressure estimation methods for use in modelling the formation of atmospheric organic aerosol, Atmos. Chem. Phys., 10, 749–767, https://doi.org/10.5194/acp-10-749-2010, 2010.

Bergman, T., Kerminen, V.-M., Korhonen, H., Lehtinen, K. J., Makkonen, R., Arola, A., Mielonen, T., Romakkaniemi, S., Kulmala, M., and Kokkola, H.: Evaluation of the sectional aerosol microphysics module SALSA implementation in ECHAM5-HAM aerosol-climate model, Geosci. Model Dev., 5, 845–868, https://doi.org/10.5194/gmd-5-845-2012, 2012.

Berndt, T., Herrmann, H., Sipilä, M., and Kulmala, M.: Highly Oxidized Second-Generation Products from the Gas-Phase Reaction of OH Radicals with Isoprene, J. Phys. Chem. A, 120, 10150–10159, 2016.

Canagaratna, M. R., Jimenez, J. L., Kroll, J. H., Chen, Q., Kessler, S. H., Massoli, P., Hildebrandt Ruiz, L., Fortner, E., Williams, L. R., Wilson, K. R., Surratt, J. D., Donahue, N. M., Jayne, J. T., and Worsnop, D. R.: Elemental ratio measurements of organic compounds using aerosol mass spectrometry: characterization, improved calibration, and implications, Atmos. Chem. Phys., 15, 253–272, https://doi.org/10.5194/acp-15-253-2015, 2015.

Carbone, S., Aurela, M., Saarnio, K., Saarikoski, S., Timonen, H., Frey, A., Sueper, D., Ulbrich, I. M., Jimenez, J. L., Kulmala, M., Worsnop, D. R., and Hollanon, R. E.: Wintertime aerosol chemistry in sub-Arctic urban air, Aerosol Sci. Technol., 48, 313–323, 2014.

Chen, Q., Farmer, D., Schneider, J., Zorn, S., Heald, C., Karl, T., Guenther, A., Allan, J., Robinson, N., Coe, H., Kimmel, J. R., Pauliquevis, T., Borrmann, S., Pöschl, U., Andreae, M. O., Artaxo, P., Jimenez, J. L., and Martin, S. T.: Mass spectral characterization of submicron biogenic organic particles in the Amazon Basin, Geophys. Res. Lett., 36, L20806, https://doi.org/10.1029/2009GL039880, 2009.

Claeys, M., Graham, B., Vas, G., Wang, W., Vermeylen, R., Pashynska, V., Cafmeyer, J., Guyon, P., Andreae, M. O., Artaxo, P., and Maenhaut, W.: Formation of secondary organic aerosols through photooxidation of isoprene, Science, 303, 1173–1176, 2004.

Clegg, S. L., Brimblecombe, P., and Wexler, A. S.: Thermodynamic Model of the System $H^+ - NH_4^+ - Na^+ - SO_4^{2-} - NO_3 - Cl-H_2O$ at 298.15 K, J. Phys. Chem. A, 102, 2155–2171, 1998.

Clements, A. L. and Seinfeld, J. H.: Detection and quantification of 2-methyltetrols in ambient aerosol in the southeastern United States, Atmos. Environ., 41, 1825–1830, 2007.

Cole-Filipiak, N. C., OConnor, A. E., and Elrod, M. J.: Kinetics of the hydrolysis of atmospherically relevant isoprene-derived hydroxy epoxides, Environ. Sci. Technol., 44, 6718–6723, 2010.

Compernolle, S., Ceulemans, K., and Müller, J.-F.: EVAPORATION: a new vapour pressure estimation methodfor organic molecules including non-additivity and intramolecular interactions, Atmos. Chem. Phys., 11, 9431–9450, https://doi.org/10.5194/acp-11-9431-2011, 2011.

Crounse, J. D., Paulot, F., Kjaergaard, H. G., and Wennberg, P. O.: Peroxy radical isomerization in the oxidation of isoprene, Phys. Chem. Chem. Phys., 13, 13607–13613, 2011.

Dall'Osto, M., Ceburnis, D., Martucci, G., Bialek, J., Dupuy, R., Jennings, S. G., Berresheim, H., Wenger, J., Healy, R., Facchini, M. C., Rinaldi, M., Giulianelli, L., Finessi, E., Worsnop, D., Ehn, M., Mikkilä, J., Kulmala, M., and O'Dowd, C. D.: Aerosol properties associated with air masses arriving into the North East Atlantic during the 2008 Mace Head EUCAARI intensive observing period: an overview, Atmos. Chem. Phys., 10, 8413–8435, https://doi.org/10.5194/acp-10-8413-2010, 2010.

D'Ambro, E. L., Lee, B. H., Liu, J., Shilling, J. E., Gaston, C. J., Lopez-Hilfiker, F. D., Schobesberger, S., Zaveri, R. A., Mohr, C., Lutz, A., Zhang, Z., Gold, A., Surratt, J. D., Rivera-Rios, J. C., Keutsch, F. N., and Thornton, J. A.: Molecular composition and volatility of isoprene photochemical oxidation sec-

ondary organic aerosol under low- and high-NO$_x$ conditions, Atmos. Chem. Phys., 17, 159–174, https://doi.org/10.5194/acp-17-159-2017, 2017a.

D'Ambro, E. L., Møller, K. H., Lopez-Hilfiker, F. D., Schobesberger, S., Liu, J., Shilling, J. E., Lee, B. H., Kjaergaard, H. G., and Thornton, J. A.: Isomerization of Second-Generation Isoprene Peroxy Radicals: Epoxide Formation and Implications for Secondary Organic Aerosol Yields, Environ. Sci. Technol., 51, 4978–4987, 2017b.

De Gouw, J. and Jimenez, J. L.: Organic aerosols in the Earths atmosphere, Environ. Sci. Technol., 43, 7614–7618, 2009.

Dentener, F., Kinne, S., Bond, T., Boucher, O., Cofala, J., Generoso, S., Ginoux, P., Gong, S., Hoelzemann, J. J., Ito, A., Marelli, L., Penner, J. E., Putaud, J.-P., Textor, C., Schulz, M., van der Werf, G. R., and Wilson, J.: Emissions of primary aerosol and precursor gases in the years 2000 and 1750 prescribed data-sets for AeroCom, Atmos. Chem. Phys., 6, 4321–4344, https://doi.org/10.5194/acp-6-4321-2006, 2006.

Donahue, N., Robinson, A., Stanier, C., and Pandis, S.: Coupled partitioning, dilution, and chemical aging of semivolatile organics, Environ. Sci. Technol., 40, 2635–2643, 2006.

Donahue, N. M., Robinson, A. L., and Pandis, S. N.: Atmospheric organic particulate matter: From smoke to secondary organic aerosol, Atmos. Environ., 43, 94–106, 2009.

Donahue, N. M., Epstein, S. A., Pandis, S. N., and Robinson, A. L.: A two-dimensional volatility basis set: 1. organic-aerosol mixing thermodynamics, Atmos. Chem. Phys., 11, 3303–3318, https://doi.org/10.5194/acp-11-3303-2011, 2011.

Donahue, N. M., Kroll, J. H., Pandis, S. N., and Robinson, A. L.: A two-dimensional volatility basis set – Part 2: Diagnostics of organic-aerosol evolution, Atmos. Chem. Phys., 12, 615–634, https://doi.org/10.5194/acp-12-615-2012, 2012.

Eddingsaas, N. C., VanderVelde, D. G., and Wennberg, P. O.: Kinetics and products of the acid-catalyzed ring-opening of atmospherically relevant butyl epoxy alcohols, J. Phys. Chem. A, 114, 8106–8113, 2010.

Emmons, L. K., Walters, S., Hess, P. G., Lamarque, J.-F., Pfister, G. G., Fillmore, D., Granier, C., Guenther, A., Kinnison, D., Laepple, T., Orlando, J., Tie, X., Tyndall, G., Wiedinmyer, C., Baughcum, S. L., and Kloster, S.: Description and evaluation of the Model for Ozone and Related chemical Tracers, version 4 (MOZART-4), Geosci. Model Dev., 3, 43–67, https://doi.org/10.5194/gmd-3-43-2010, 2010.

Epstein, S. A., Riipinen, I., and Donahue, N. M.: A semiempirical correlation between enthalpy of vaporization and saturation concentration for organic aerosol, Environ. Sci. Technol., 44, 743–748, 2009.

Ervens, B. and Volkamer, R.: Glyoxal processing by aerosol multiphase chemistry: towards a kinetic modeling framework of secondary organic aerosol formation in aqueous particles, Atmos. Chem. Phys., 10, 8219–8244, https://doi.org/10.5194/acp-10-8219-2010, 2010.

Farina, S. C., Adams, P. J., and Pandis, S. N.: Modeling global secondary organic aerosol formation and processing with the volatility basis set: Implications for anthropogenic secondary organic aerosol, J. Geophys. Res.-Atmos., 115, D09202, https://doi.org/10.1029/2009JD013046, 2010.

Fröhlich-Nowoisky, J., Kampf, C. J., Weber, B., Huffman, J. A., Pöhlker, C., Andreae, M. O., Lang-Yona, N., Burrows, S. M.,

Gunthe, S. S., Elbert, W., et al.: Bioaerosols in the Earth system: Climate, health, and ecosystem interactions, Atmos. Res., 182, 346–376, 2016.

Fu, T.-M., Jacob, D. J., Wittrock, F., Burrows, J. P., Vrekoussis, M., and Henze, D. K.: Global budgets of atmospheric glyoxal and methylglyoxal, and implications for formation of secondary organic aerosols, J. Geophys. Res.-Atmos., 113, F15303, https://doi.org/10.1029/2007JD009505, 2008.

Fuzzi, S., Baltensperger, U., Carslaw, K., Decesari, S., Denier van der Gon, H., Facchini, M. C., Fowler, D., Koren, I., Langford, B., Lohmann, U., Nemitz, E., Pandis, S., Riipinen, I., Rudich, Y., Schaap, M., Slowik, J. G., Spracklen, D. V., Vignati, E., Wild, M., Williams, M., and Gilardoni, S.: Particulate matter, air quality and climate: lessons learned and future needs, Atmos. Chem. Phys., 15, 8217–8299, https://doi.org/10.5194/acp-15-8217-2015, 2015.

Gaston, C. J., Riedel, T. P., Zhang, Z., Gold, A., Surratt, J. D., and Thornton, J. A.: Reactive uptake of an isoprene-derived epoxydiol to submicron aerosol particles, Environ. Sci. Technol., 48, 11178–11186, 2014.

Ghan, S. J. and Schwartz, S. E.: Aerosol properties and processes: A path from field and laboratory measurements to global climate models, B. Am. Meteorol. Soc., 88, 1059–1083, 2007.

Goldstein, A. H. and Galbally, I. E.: Known and unexplored organic constituents in the earth's atmosphere, Environ. Sci. Technol., 41, 1514–1521, 2007.

Guenther, A., Karl, T., Harley, P., Wiedinmyer, C., Palmer, P. I., and Geron, C.: Estimates of global terrestrial isoprene emissions using MEGAN (Model of Emissions of Gases and Aerosols from Nature), Atmos. Chem. Phys., 6, 3181–3210, https://doi.org/10.5194/acp-6-3181-2006, 2006.

Hallquist, M., Wenger, J. C., Baltensperger, U., Rudich, Y., Simpson, D., Claeys, M., Dommen, J., Donahue, N. M., George, C., Goldstein, A. H., Hamilton, J. F., Herrmann, H., Hoffmann, T., Iinuma, Y., Jang, M., Jenkin, M. E., Jimenez, J. L., Kiendler-Scharr, A., Maenhaut, W., McFiggans, G., Mentel, Th. F., Monod, A., Prévôt, A. S. H., Seinfeld, J. H., Surratt, J. D., Szmigielski, R., and Wildt, J.: The formation, properties and impact of secondary organic aerosol: current and emerging issues, Atmos. Chem. Phys., 9, 5155–5236, https://doi.org/10.5194/acp-9-5155-2009, 2009.

Heald, C. L., Jacob, D. J., Park, R. J., Russell, L. M., Huebert, B. J., Seinfeld, J. H., Liao, H., and Weber, R. J.: A large organic aerosol source in the free troposphere missing from current models, Geophys. Res. Lett., 32, L18809, https://doi.org/10.1029/2005GL023831, 2005.

Henrot, A.-J., Stanelle, T., Schröder, S., Siegenthaler, C., Taraborrelli, D., and Schultz, M. G.: Implementation of the MEGAN (v2.1) biogenic emission model in the ECHAM6-HAMMOZ chemistry climate model, Geosci. Model Dev., 10, 903–926, https://doi.org/10.5194/gmd-10-903-2017, 2017.

Hodzic, A., Madronich, S., Kasibhatla, P. S., Tyndall, G., Aumont, B., Jimenez, J. L., Lee-Taylor, J., and Orlando, J.: Organic photolysis reactions in tropospheric aerosols: effect on secondary organic aerosol formation and lifetime, Atmos. Chem. Phys., 15, 9253–9269, https://doi.org/10.5194/acp-15-9253-2015, 2015.

Hodzic, A., Kasibhatla, P. S., Jo, D. S., Cappa, C. D., Jimenez, J. L., Madronich, S., and Park, R. J.: Rethinking the global secondary organic aerosol (SOA) budget: stronger production, faster

removal, shorter lifetime, Atmos. Chem. Phys., 16, 7917–7941, https://doi.org/10.5194/acp-16-7917-2016, 2016.

IPCC: Annex I: Atlas of Global and Regional Climate Projections, Cambridge University Press, Cambridge, UK, New York, NY, USA, book section AI, 1311–1394, https://doi.org/10.1017/CBO9781107415324.029, 2013.

Jimenez, J., Canagaratna, M., Donahue, N., et al.: Evolution of organic aerosols in the atmosphere, Science, 326, 1525–1529, 2009.

Jülich Supercomputing Centre: JURECA: General-purpose supercomputer at Jülich Supercomputing Centre, J. Large-scale Res. Fac., 2, A62, https://doi.org/10.17815/jlsrf-2-121, 2016.

Kanakidou, M., Seinfeld, J. H., Pandis, S. N., Barnes, I., Dentener, F. J., Facchini, M. C., Van Dingenen, R., Ervens, B., Nenes, A., Nielsen, C. J., Swietlicki, E., Putaud, J. P., Balkanski, Y., Fuzzi, S., Horth, J., Moortgat, G. K., Winterhalter, R., Myhre, C. E. L., Tsigaridis, K., Vignati, E., Stephanou, E. G., and Wilson, J.: Organic aerosol and global climate modelling: a review, Atmos. Chem. Phys., 5, 1053–1123, https://doi.org/10.5194/acp-5-1053-2005, 2005.

Kavouras, I. G., Mihalopoulos, N., and Stephanou, E. G.: Secondary organic aerosol formation vs primary organic aerosol emission: In situ evidence for the chemical coupling between monoterpene acidic photooxidation products and new particle formation over forests, Environ. Sci. Technol., 33, 1028–1037, 1999.

Kinnison, D., Brasseur, G., Walters, S., Garcia, R., Marsh, D., Sassi, F., Harvey, V., Randall, C., Emmons, L., Lamarque, J., Hess, P., Orlando, J. J., Tie, X. X., Randel, W., Pan, L. L., Gettelman, A., Granier, C., Diehl, T., Niemeier, U., and Simmons, A. J.: Sensitivity of chemical tracers to meteorological parameters in the MOZART-3 chemical transport model, J. Geophys. Res.-Atmos., 112, D20302, https://doi.org/10.1029/2006JD007879, 2007.

Kokkola, H., Korhonen, H., Lehtinen, K. E. J., Makkonen, R., Asmi, A., Järvenoja, S., Anttila, T., Partanen, A.-I., Kulmala, M., Järvinen, H., Laaksonen, A., and Kerminen, V.-M.: SALSA – a Sectional Aerosol module for Large Scale Applications, Atmos. Chem. Phys., 8, 2469–2483, https://doi.org/10.5194/acp-8-2469-2008, 2008.

Kokkola, H., Kühn, T., Laakso, A., Bergman, T., Lehtinen, K. E. J., Mielonen, T., Arola, A., Stadtler, S., Korhonen, H., Ferrachat, S., Lohmann, U., Neubauer, D., Tegen, I., Siegenthaler-Le Drian, C., Schultz, M. G., Bey, I., Stier, P., Daskalakis, N., Heald, C. L., and Romakkaniemi, S.: SALSA2.0: The sectional aerosol module of the aerosol-chemistry-climate model ECHAM6.3.0-HAM2.3-MOZ1.0, Geosci. Model Dev. Discuss., https://doi.org/10.5194/gmd-2018-47, in review, 2018.

Kourtchev, I., Ruuskanen, T., Maenhaut, W., Kulmala, M., and Claeys, M.: Observation of 2-methyltetrols and related photo-oxidation products of isoprene in boreal forest aerosols from Hyytiälä, Finland, Atmos. Chem. Phys., 5, 2761–2770, https://doi.org/10.5194/acp-5-2761-2005, 2005.

Kroll, J. H., Ng, N. L., Murphy, S. M., Flagan, R. C., and Seinfeld, J. H.: Secondary organic aerosol formation from isoprene photooxidation, Environ. Sci. Technol., 40, 1869–1877, 2006.

Kühn, T., Merikanto, J., Mielonen, T., Stadtler, S., Hienola, A., Korhonen, H., Ferrachat, S., Lohmann, U., Neubauer, D., Tegen, I., Siegenthaler-Le Drian, C., Wahl, S., Schultz, M. G., Rast, S., Schmidt, H., Stier, P., Lehtinen, K., and Kokkola, H.: SALSA2.0 part2: Implementation of a volatility basis set to model forma-

tion of secondary organic aerosol, Geosci. Model Dev., in preparation, 2018.

Kurten, T., Tiusanen, K., Roldin, P., Rissanen, M., Luy, J.-N., Boy, M., Ehn, M., and Donahue, N.: $\alpha$-Pinene autoxidation products may not have extremely low saturation vapor pressures despite high O : C ratios, J. Phys. Chem. A, 120, 2569–2582, 2016.

Lakey, P. S., Berkemeier, T., Tong, H., Arangio, A. M., Lucas, K., Pöschl, U., and Shiraiwa, M.: Chemical exposure-response relationship between air pollutants and reactive oxygen species in the human respiratory tract, Sci. Rep.-UK, 6, 32916, https://doi.org/10.1038/srep32916, 2016.

Lal, V., Khalizov, A. F., Lin, Y., Galvan, M. D., Connell, B. T., and Zhang, R.: Heterogeneous reactions of epoxides in acidic media, J. Phys. Chem. A, 116, 6078–6090, 2012.

Lamarque, J.-F., Bond, T. C., Eyring, V., Granier, C., Heil, A., Klimont, Z., Lee, D., Liousse, C., Mieville, A., Owen, B., Schultz, M. G., Shindell, D., Smith, S. J., Stehfest, E., Van Aardenne, J., Cooper, O. R., Kainuma, M., Mahowald, N., McConnell, J. R., Naik, V., Riahi, K., and van Vuuren, D. P.: Historical (1850–2000) gridded anthropogenic and biomass burning emissions of reactive gases and aerosols: methodology and application, Atmos. Chem. Phys., 10, 7017–7039, https://doi.org/10.5194/acp-10-7017-2010, 2010.

Lelieveld, J., Gromov, S., Pozzer, A., and Taraborrelli, D.: Global tropospheric hydroxyl distribution, budget and reactivity, Atmos. Chem. Phys., 16, 12477–12493, https://doi.org/10.5194/acp-16-12477-2016, 2016.

Li, N., Fu, T.-M., Cao, J., Lee, S., Huang, X.-F., He, L.-Y., Ho, K.-F., Fu, J. S., and Lam, Y.-F.: Sources of secondary organic aerosols in the Pearl River Delta region in fall: Contributions from the aqueous reactive uptake of dicarbonyls, Atmos. Environ., 76, 200–207, 2013.

Liggio, J., Li, S.-M., and McLaren, R.: Heterogeneous reactions of glyoxal on particulate matter: Identification of acetals and sulfate esters, Environ. Sci. Technol., 39, 1532–1541, 2005a.

Liggio, J., Li, S.-M., and McLaren, R.: Reactive uptake of glyoxal by particulate matter, J. Geophys. Res.-Atmos., 110, D10304, https://doi.org/10.1029/2004JD005113, 2005b.

Lin, G., Penner, J. E., Sillman, S., Taraborrelli, D., and Lelieveld, J.: Global modeling of SOA formation from dicarbonyls, epoxides, organic nitrates and peroxides, Atmos. Chem. Phys., 12, 4743–4774, https://doi.org/10.5194/acp-12-4743-2012, 2012.

Lin, S.-J. and Rood, R. B.: Multidimensional flux-form semi-Lagrangian transport schemes, Mon. Weather Rev., 124, 2046–2070, 1996.

Lin, Y.-H., Knipping, E. M., Edgerton, E. S., Shaw, S. L., and Surratt, J. D.: Investigating the influences of $SO_2$ and $NH_3$ levels on isoprene-derived secondary organic aerosol formation using conditional sampling approaches, Atmos. Chem. Phys., 13, 8457–8470, https://doi.org/10.5194/acp-13-8457-2013, 2013a.

Lin, Y.-H., Zhang, H., Pye, H. O., Zhang, Z., Marth, W. J., Park, S., Arashiro, M., Cui, T., Budisulistiorini, S. H., Sexton, K. G., Vizuete, W., Xie, Y., Luecken, D. J., Piletic, I. R., Edney, E. O., Bartolotti, L. J., Gold, A., and Surratt, J. D.: Epoxide as a precursor to secondary organic aerosol formation from isoprene photooxidation in the presence of nitrogen oxides, P. Natl. Acad. Sci. USA, 110, 6718–6723, 2013b.

Liu, J., DAmbro, E. L., Lee, B. H., Lopez-Hilfiker, F. D., Zaveri, R. A., Rivera-Rios, J. C., Keutsch, F. N., Iyer, S., Kurten, T.,

Zhang, Z., Gold, A., Surratt, J. D., Shilling, J. E., and Thornton, J. A.: Efficient isoprene secondary organic aerosol formation from a non-IEPOX pathway, Environ. Sci. Technol., 50, 9872–9880, 2016.

Lopez-Hilfiker, F., Mohr, C., DAmbro, E. L., Lutz, A., Riedel, T. P., Gaston, C. J., Iyer, S., Zhang, Z., Gold, A., Surratt, J. D., Lee, B. H., Kurten, T., Hu, W. W., Jimenez, J., Hallquist, M., and Thornton, J. A.: Molecular composition and volatility of organic aerosol in the Southeastern US: implications for IEPOX derived SOA, Environ. Sci. Technol., 50, 2200–2209, 2016.

Malecha, K. T. and Nizkorodov, S. A.: Photodegradation of secondary organic aerosol particles as a source of small, oxygenated volatile organic compounds, Environ. Sci. Technol., 50, 9990–9997, 2016.

Marais, E. A., Jacob, D. J., Jimenez, J. L., Campuzano-Jost, P., Day, D. A., Hu, W., Krechmer, J., Zhu, L., Kim, P. S., Miller, C. C., Fisher, J. A., Travis, K., Yu, K., Hanisco, T. F., Wolfe, G. M., Arkinson, H. L., Pye, H. O. T., Froyd, K. D., Liao, J., and McNeill, V. F.: Aqueous-phase mechanism for secondary organic aerosol formation from isoprene: application to the southeast United States and co-benefit of $SO_2$ emission controls, Atmos. Chem. Phys., 16, 1603–1618, https://doi.org/10.5194/acp-16-1603-2016, 2016.

Martin, S. T., Andreae, M. O., Althausen, D., Artaxo, P., Baars, H., Borrmann, S., Chen, Q., Farmer, D. K., Guenther, A., Gunthe, S. S., Jimenez, J. L., Karl, T., Longo, K., Manzi, A., Müller, T., Pauliquevis, T., Petters, M. D., Prenni, A. J., Pöschl, U., Rizzo, L. V., Schneider, J., Smith, J. N., Swietlicki, E., Tota, J., Wang, J., Wiedensohler, A., and Zorn, S. R.: An overview of the Amazonian Aerosol Characterization Experiment 2008 (AMAZE-08), Atmos. Chem. Phys., 10, 11415–11438, https://doi.org/10.5194/acp-10-11415-2010, 2010.

McFiggans, G., Topping, D. O., and Barley, M. H.: The sensitivity of secondary organic aerosol component partitioning to the predictions of component properties – Part 1: A systematic evaluation of some available estimation techniques, Atmos. Chem. Phys., 10, 10255–10272, https://doi.org/10.5194/acp-10-10255-2010, 2010.

McNeill, V. F., Woo, J. L., Kim, D. D., Schwier, A. N., Wannell, N. J., Sumner, A. J., and Barakat, J. M.: Aqueous-phase secondary organic aerosol and organosulfate formation in atmospheric aerosols: a modeling study, Environ. Sci. Technol., 46, 8075–8081, 2012.

Nannoolal, Y., Rarey, J., Ramjugernath, D., and Cordes, W.: Estimation of pure component properties: Part 1. Estimation of the normal boiling point of non-electrolyte organic compounds via group contributions and group interactions, Fluid Phase Equilibr., 226, 45–63, 2004.

Nannoolal, Y., Rarey, J., and Ramjugernath, D.: Estimation of pure component properties: Part 3. Estimation of the vapor pressure of non-electrolyte organic compounds via group contributions and group interactions, Fluid Phase Equilibr., 269, 117–133, 2008.

Nölscher, A., Butler, T., Auld, J., Veres, P., Muñoz, A., Taraborrelli, D., Vereecken, L., Lelieveld, J., and Williams, J.: Using total OH reactivity to assess isoprene photooxidation via measurement and model, Atmos. Environ., 89, 453–463, 2014.

Nozière, B., González, N. J., Borg-Karlson, A.-K., Pei, Y., Redeby, J. P., Krejci, R., Dommen, J., Prévôt, A. S., and Anthonsen, T.: Atmospheric chemistry in stereo: A new look at secondary or-

ganic aerosols from isoprene, Geophys. Res. Lett., 38, L11807, https://doi.org/10.1029/2011GL047323, 2011.

O'Donnell, D., Tsigaridis, K., and Feichter, J.: Estimating the direct and indirect effects of secondary organic aerosols using ECHAM5-HAM, Atmos. Chem. Phys., 11, 8635–8659, https://doi.org/10.5194/acp-11-8635-2011, 2011.

Odum, J. R., Hoffmann, T., Bowman, F., Collins, D., Flagan, R. C., and Seinfeld, J. H.: Gas/particle partitioning and secondary organic aerosol yields, Environ. Sci. Technol., 30, 2580–2585, 1996.

OMeara, S., Booth, A. M., Barley, M. H., Topping, D., and McFiggans, G.: An assessment of vapour pressure estimation methods, Phys. Chem. Chem. Phys., 16, 19453–19469, 2014.

Pandis, S. N., Harley, R. A., Cass, G. R., and Seinfeld, J. H.: Secondary organic aerosol formation and transport, Atmos. Environ. A-Gen., 26, 2269–2282, 1992.

Pankow, J. F.: An absorption model of gas/particle partitioning of organic compounds in the atmosphere, Atmos. Environ., 28, 185–188, 1994.

Paulot, F., Crounse, J. D., Kjaergaard, H. G., Kürten, A., Clair, J. M. S., Seinfeld, J. H., and Wennberg, P. O.: Unexpected epoxide formation in the gas-phase photooxidation of isoprene, Science, 325, 730–733, 2009.

Pöschl, U., Martin, S., Sinha, B., Chen, Q., Gunthe, S., Huffman, J., Borrmann, S., Farmer, D., Garland, R., Helas, G., Jimenez, J. L., King, S. M., Manzi, A., Mikhailov, E., Pauliquevis, T., Petters, M. D., Prenni, A. J., Roldin, P., Rose, D., Schneider, J., Su, H., Zorn, S. R., Artaxo, P., and Andreae, M. O.: Rainforest aerosols as biogenic nuclei of clouds and precipitation in the Amazon, Science, 329, 1513–1516, 2010.

Pye, H. O., Pinder, R. W., Piletic, I. R., Xie, Y., Capps, S. L., Lin, Y.-H., Surratt, J. D., Zhang, Z., Gold, A., Luecken, D. J., Hutzell, W. T., Jaoui, M., Offenberg, J. H., Kleindienst, T. E., Lewandowski, M., and Edney, E. O.: Epoxide pathways improve model predictions of isoprene markers and reveal key role of acidity in aerosol formation, Environ. Sci. Technol., 47, 11056–11064, 2013.

Riedel, T. P., Lin, Y.-H., Budisulistiorini, S. H., Gaston, C. J., Thornton, J. A., Zhang, Z., Vizuete, W., Gold, A., and Surratt, J. D.: Heterogeneous reactions of isoprene-derived epoxides: reaction probabilities and molar secondary organic aerosol yield estimates, Environ. Sci. Tech. Let., 2, 38–42, 2015.

Riva, M., Budisulistiorini, S. H., Chen, Y., Zhang, Z., DAmbro, E. L., Zhang, X., Gold, A., Turpin, B. J., Thornton, J. A., Canagaratna, M. R., and Surrat J. D.: Chemical characterization of secondary organic aerosol from oxidation of isoprene hydroxyhydroperoxides, Environ. Sci. Technol., 50, 9889–9899, 2016.

Saarikoski, S., Carbone, S., Decesari, S., Giulianelli, L., Angelini, F., Canagaratna, M., Ng, N. L., Trimborn, A., Facchini, M. C., Fuzzi, S., Hillamo, R., and Worsnop, D.: Chemical characterization of springtime submicrometer aerosol in Po Valley, Italy, Atmos. Chem. Phys., 12, 8401–8421, https://doi.org/10.5194/acp-12-8401-2012, 2012.

Schultz, M. G., Stadtler, S., Schröder, S., Taraborrelli, D., Franco, B., Krefting, J., Henrot, A., Ferrachat, S., Lohmann, U., Neubauer, D., Siegenthaler-Le Drian, C., Wahl, S., Kokkola, H., Kühn, T., Rast, S., Schmidt, H., Stier, P., Kinnison, D., Tyndall, G. S., Orlando, J. J., and Wespes, C.: The chemistry–climate model ECHAM6.3-HAM2.3-MOZ1.0, Geosci. Model Dev., 11, 1695–1723, https://doi.org/10.5194/gmd-11-1695-2018, 2018.

Schwartz, S. E.: Mass-transport considerations pertinent to aqueous phase reactions of gases in liquid-water clouds, in: Chemistry of multiphase atmospheric systems, Springer, 415–471, 1986.

Seinfeld, J. H. and Pankow, J. F.: Organic atmospheric particulate material, Annu. Rev. Phys. Chem., 54, 121–140, 2003.

Shiraiwa, M., Li, Y., Tsimpidi, A. P., Karydis, V. A., Berkemeier, T., Pandis, S. N., Lelieveld, J., Koop, T., and Pöschl, U.: Global distribution of particle phase state in atmospheric secondary organic aerosols, Nat. Commun., 8, 15002, https://doi.org/10.1038/ncomms15002, 2017.

Stadtler, S.: Isoprene secondary organic aerosol in a global chemistry climate model, Phd thesis, University of Bonn, Bonn, Germany, 2018.

Stadtler, S., Simpson, D., Schröder, S., Taraborrelli, D., Bott, A., and Schultz, M.: Ozone impacts of gas–aerosol uptake in global chemistry transport models, Atmos. Chem. Phys., 18, 3147–3171, https://doi.org/10.5194/acp-18-3147-2018, 2018a.

Stadtler, S., Kühn, T., Schröder, S., Taraborrelli, D., Schultz, M. G., and Kokkola, H.: Results from Isoprene derived secondary organic aerosol in the global aerosol-chemistry-climate model ECHAM6.3.0-HAM2.3-MOZ1.0 https://doi.org/10.23728/b2share.426c8d3200a54193886fed954b6097c2, 2018b.

Stein, O., Flemming, J., Inness, A., Kaiser, J. W., and Schultz, M. G.: Global reactive gases forecasts and reanalysis in the MACC project, J. Integr. Environ. Sci., 9, 57–70, 2012.

Steinbrecher, R., Smiatek, G., Köble, R., Seufert, G., Theloke, J., Hauff, K., Ciccioli, P., Vautard, R., and Curci, G.: Intra-and inter-annual variability of VOC emissions from natural and semi-natural vegetation in Europe and neighbouring countries, Atmos. Environ., 43, 1380–1391, 2009.

Stevens, B., Giorgetta, M., Esch, M., Mauritsen, T., Crueger, T., Rast, S., Salzmann, M., Schmidt, H., Bader, J., Block, K., Brokopf, R., Fast, I., Kinne, S., Kornblueh, L., Lohmann, U., Pincus, R., Reichler T., and Roeckner, E.: Atmospheric component of the MPI-M Earth System Model: ECHAM6, J. Adv. Model Earth, Sy., 5, 146–172, 2013.

Stier, P., Feichter, J., Kinne, S., Kloster, S., Vignati, E., Wilson, J., Ganzeveld, L., Tegen, I., Werner, M., Balkanski, Y., Schulz, M., Boucher, O., Minikin, A., and Petzold, A.: The aerosol-climate model ECHAM5-HAM, Atmos. Chem. Phys., 5, 1125–1156, https://doi.org/10.5194/acp-5-1125-2005, 2005.

Surratt, J. D., Murphy, S. M., Kroll, J. H., Ng, N. L., Hildebrandt, L., Sorooshian, A., Szmigielski, R., Vermeylen, R., Maenhaut, W., Claeys, M., Flagan, R. C., and Seinfeld, J. H.: Chemical composition of secondary organic aerosol formed from the photooxidation of isoprene, J. Phys. Chem. A, 110, 9665–9690, 2006.

Surratt, J. D., Kroll, J. H., Kleindienst, T. E., Edney, E. O., Claeys, M., Sorooshian, A., Ng, N. L., Offenberg, J. H., Lewandowski, M., Jaoui, M., Flagan, R. C., and Seinfeld, J. H.: Evidence for organosulfates in secondary organic aerosol, Environ. Sci. Technol., 41, 517–527, 2007a.

Surratt, J. D., Lewandowski, M., Offenberg, J. H., Jaoui, M., Kleindienst, T. E., Edney, E. O., and Seinfeld, J. H.: Effect of acidity on secondary organic aerosol formation from isoprene, Environ. Sci. Technol., 41, 5363–5369, 2007b.

Surratt, J. D., Chan, A. W., Eddingsaas, N. C., Chan, M., Loza, C. L., Kwan, A. J., Hersey, S. P., Flagan, R. C., Wennberg, P. O., and Seinfeld, J. H.: Reactive intermediates revealed in secondary organic aerosol formation from isoprene, P. Natl. Acad. Sci. USA, 107, 6640–6645, 2010.

Taraborrelli, D., Lawrence, M. G., Butler, T. M., Sander, R., and Lelieveld, J.: Mainz Isoprene Mechanism 2 (MIM2): an isoprene oxidation mechanism for regional and global atmospheric modelling, Atmos. Chem. Phys., 9, 2751–2777, https://doi.org/10.5194/acp-9-2751-2009, 2009.

Taraborrelli, D., Lawrence, M., Crowley, J., Dillon, T., Gromov, S., Groß, C., Vereecken, L., and Lelieveld, J.: Hydroxyl radical buffered by isoprene oxidation over tropical forests, Nat. Geosci., 5, 190–193, 2012.

Timonen, H., Aurela, M., Carbone, S., Saarnio, K., Saarikoski, S., Mäkelä, T., Kulmala, M., Kerminen, V.-M., Worsnop, D. R., and Hillamo, R.: High time-resolution chemical characterization of the water-soluble fraction of ambient aerosols with PILS-TOC-IC and AMS, Atmos. Meas. Tech., 3, 1063–1074, https://doi.org/10.5194/amt-3-1063-2010, 2010.

Topping, D., Barley, M., Bane, M. K., Higham, N., Aumont, B., Dingle, N., and McFiggans, G.: UManSysProp v1.0: an online and open-source facility for molecular property prediction and atmospheric aerosol calculations, Geosci. Model Dev., 9, 899–914, https://doi.org/10.5194/gmd-9-899-2016, 2016.

Tsigaridis, K. and Kanakidou, M.: Global modelling of secondary organic aerosol in the troposphere: a sensitivity analysis, Atmos. Chem. Phys., 3, 1849–1869, https://doi.org/10.5194/acp-3-1849-2003, 2003.

Tsigaridis, K., Daskalakis, N., Kanakidou, M., Adams, P. J., Artaxo, P., Bahadur, R., Balkanski, Y., Bauer, S. E., Bellouin, N., Benedetti, A., Bergman, T., Berntsen, T. K., Beukes, J. P., Bian, H., Carslaw, K. S., Chin, M., Curci, G., Diehl, T., Easter, R. C., Ghan, S. J., Gong, S. L., Hodzic, A., Hoyle, C. R., Iversen, T., Jathar, S., Jimenez, J. L., Kaiser, J. W., Kirkevåg, A., Koch, D., Kokkola, H., Lee, Y. H., Lin, G., Liu, X., Luo, G., Ma, X., Mann, G. W., Mihalopoulos, N., Morcrette, J.-J., Müller, J.-F., Myhre, G., Myriokefalitakis, S., Ng, N. L., O'Donnell, D., Penner, J. E., Pozzoli, L., Pringle, K. J., Russell, L. M., Schulz, M., Sciare, J., Seland, Ø., Shindell, D. T., Sillman, S., Skeie, R. B., Spracklen, D., Stavrakou, T., Steenrod, S. D., Takemura, T., Tiitta, P., Tilmes, S., Tost, H., van Noije, T., van Zyl, P. G., von Salzen, K., Yu, F., Wang, Z., Wang, Z., Zaveri, R. A., Zhang, H., Zhang, K., Zhang, Q., and Zhang, X.: The AeroCom evaluation and intercomparison of organic aerosol in global models, Atmos. Chem. Phys., 14, 10845–10895, https://doi.org/10.5194/acp-14-10845-2014, 2014.

Volkamer, R., Jimenez, J. L., San Martini, F., Dzepina, K., Zhang, Q., Salcedo, D., Molina, L. T., Worsnop, D. R., and Molina, M. J.: Secondary organic aerosol formation from anthropogenic air pollution: Rapid and higher than expected, Geophys. Res. Lett., 33, L17811, https://doi.org/10.1029/2006GL026899, 2006.

Volkamer, R., San Martini, F., Molina, L. T., Salcedo, D., Jimenez, J. L., and Molina, M. J.: A missing sink for gas-phase glyoxal in Mexico City: Formation of secondary organic aerosol, Geophys. Res. Lett., 34, L19807, https://doi.org/10.1029/2007GL030752, 2007.

Washenfelder, R., Young, C., Brown, S., Angevine, W., Atlas, E., Blake, D., Bon, D., Cubison, M., De Gouw, J., Dusanter, S., Flynn, J., Gilman, J. B., Graus, M., Griffith, S., Grossberg, N., Hayes, P. L., Jimenez, J. L., Kuster, W. C., Lefer, B. L., Pollack, I. B., Ryerson, T. B., Stark, H., Stevens, P. S., and Trainer, M. K.:

The glyoxal budget and its contribution to organic aerosol for Los Angeles, California, during CalNex 2010, J. Geophys. Res.-Atmos., 116, D00V02, https://doi.org/10.1029/2011JD016314, 2011.

Waxman, E. M., Dzepina, K., Ervens, B., Lee-Taylor, J., Aumont, B., Jimenez, J. L., Madronich, S., and Volkamer, R.: Secondary organic aerosol formation from semi-and intermediate-volatility organic compounds and glyoxal: Relevance of O / C as a tracer for aqueous multiphase chemistry, Geophys. Res. Lett., 40, 978–982, 2013.

Woo, J. L. and McNeill, V. F.: simpleGAMMA v1.0 – a reduced model of secondary organic aerosol formation in the aqueous aerosol phase (aaSOA), Geosci. Model Dev., 8, 1821–1829, https://doi.org/10.5194/gmd-8-1821-2015, 2015.

Xu, L., Guo, H., Boyd, C. M., Klein, M., Bougiatioti, A., Cerully, K. M., Hite, J. R., Isaacman-VanWertz, G., Kreisberg, N. M., Knote, C., Olson, K., Koss, A., Goldstein, A. H., Hering, S. V., de Gouw, J., Baumann, K., Lee, S.-H., Nenes, A., Weber, R. J., and Ng, N. L.: Effects of anthropogenic emissions on aerosol formation from isoprene and monoterpenes in the southeastern United States, P. Natl. Acad. Sci. USA, 112, 37–42, 2015.

Zhang, Q., Jimenez, J., Canagaratna, M., et al.: Ubiquity and dominance of oxygenated species in organic aerosols in anthropogenically-influenced Northern Hemisphere midlatitudes, Geophys. Res. Lett., 34, L13801, https://doi.org/10.1029/2007GL029979, 2007.

Zhang, Q., Parworth, C., Lechner, M., and Jimenez, J.: Aerosol Mass Spectrometer Global Database, https://doi.org/10.6084/m9.figshare.3486719, last access: 22 September 2017.